

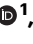




Type III interferon primes pDCs for TLR7 activation and antagonizes immune suppression mediated by TGF- β and PGE2

Received: 19 July 2023

Accepted: 12 March 2025

Published online: 28 March 2025

 Check for updates

Candice Sakref^{1,2,8}, Alexis Saby^{1,8}, Céline Rodriguez^{1,3}, Maude Ardin^{1,4}, Lyvia Moudombi¹, Anne-Claire Doffin¹, Elisa Gobbini¹, Aurélien Voissiere ¹, Laurie Besson^{1,5}, Léo Laoubi¹, Jan Böttcher ^{6,7}, Stéphane Depil^{1,5}, Margaux Hubert ^{1,4,5}, Nathalie Bendriss-Vermare ^{1,3}, Christophe Caux^{1,2,3} & Jenny Valladeau-Guilemond ^{1,2} ✉

Conventional dendritic cell and plasmacytoid dendritic cell (pDC) subsets have specialized functions that can be modulated by the tumor micro-environment, and produce different interferons that are central to antitumor immune responses. While the function of type I interferons in tumor immunity is well characterized, that of type III interferons produced by type 1 conventional dendritic cells in the tumor microenvironment remains unclear. Here we demonstrate in vitro that type III interferons orchestrate pDC survival, activation and TLR7 expression in the blood, thereby enhancing pDC responses to a TLR7 ligand. Moreover, we show that tumor-associated pDCs express the highest level of IFNLR1, and that these immune cell subsets are the most responsive to IFN-III. Importantly, type III interferons prevent the inhibition of pDCs induced by TGF- β or PGE2 in tumor soluble milieu from patients to restores production of IFN- α in pDCs. With TGF- β or PGE2 having pleiotropic functions in immune regulation, our results thus implicate IFN-III-mediated immune modulation to have broad impact on various pathological situations.

pDCs can be distinguished from conventional dendritic cells (cDC) by their lack of CD11c and the surface expression of BDCA2/CD303 and IL-3 Receptor (CD123). Their main function is to produce high amounts of type I interferon (IFN-I) after TLR7 or TLR9 engagement by viral ssRNA and ODNs CpG, respectively^{1,2}. IFN-I produced by pDCs was shown to induce antiviral and antitumor responses in epithelial cells and immune cells^{3,4}, which has led to the approval of IFN-I derivatives, namely IFN- α 2A and IFN- α 2B, as treatments for several malignancies⁵. In cancer, an IFN-I signature in the tumor microenvironment (TME) was correlated with “hot tumors”, characterized by a strong immune infiltrate and a

better response to immunotherapies⁶. Conversely, the downregulation of IFN-I receptor (IFNARI) is associated with a poor clinical outcome and tumor progression in melanoma⁷, breast and colorectal cancers^{8,9}.

The precise role of pDCs within the TME remains unclear. While pDC infiltration within tumors was correlated with positive prognosis in colorectal and pancreatic cancers, pDCs were associated with a negative prognosis in ovarian cancer. In breast cancer, they were associated with a positive or negative prognosis¹⁰. In this context, we and others have demonstrated that pDCs are dysregulated in the TME, displaying a particularly poor capacity to secrete IFN- α ^{11–13}. This was

¹Centre de Recherche en Cancérologie de Lyon, Centre Léon Bérard, Université de Lyon, Université Claude Bernard Lyon 1, PLASCAN, INSERM 1052, CNRS, 5286 Lyon, France. ²LabEx DEVweCAN, Lyon, France. ³Laboratory of Cancer Immunotherapy of Lyon (LICL), Centre Léon Bérard, Lyon, France. ⁴Synergie Lyon Cancer, Plateforme de bio-informatique ‘Gilles Thomas’, Centre Léon Bérard, Lyon, France. ⁵Centre Léon Bérard, F-, Lyon, France. ⁶Department of Experimental Immunology, Institute of Immunology, University of Tübingen, Tübingen, Germany. ⁷Institute of Molecular Immunology, TUM University Hospital, School of Medicine and Health, Technical University of Munich (TUM), Munich, Germany. ⁸These authors contributed equally: Candice Sakref, Alexis Saby.

✉ e-mail: jenny.valladeau-guilemond@lyon.unicancer.fr

mostly due to TGF- β which downregulates TLR9¹⁴ and IFR7 expression, and reduces IRF7 translocation to the nucleus¹⁵, as well as PGE2 which is also able to inhibit pDC activation^{14,16}. Thus, the use of TLR to reactivate an antitumor immune response¹⁷ has to take into account this immunosuppression.

In parallel, our team has recently shown that the cDC1 population contributes to antitumor responses through the production of Type III interferon (IFN-III) (also known as IFN- λ)¹⁸. IFN-III in humans include four subtypes, IFN- λ 1 (IL-29), IFN- λ 2 (IL-28A), IFN- λ 3 (IL-28B), and IFN- λ 4. In mice, the type III IFN family consists of IFN- λ 2 and IFN- λ 3, where IFN- λ 1 is a pseudogene and the genomic region encoding IFN- λ 4 is absent¹⁹. IFN-III first interacts with the IFNLR1 chain, that recruits the IL-10R β chain to form the heterodimer IFN-Lambda Receptor (IFNLR). Once IFN-III interacts with IFNLR complex, the intracellular signaling pathway resembles that of the IFN-I pathway. JAK1 and TYK2 tyrosine kinases induce STAT1 and STAT2 phosphorylation which both bind to IRF9 and create the ISGF3 complex²⁰. ISGF3 then translocates to the nucleus where it binds interferon-stimulated response elements (ISRE) to activate the transcription of several interferon-stimulated genes (ISGs). In addition to the dominant JAK-STAT signaling response, type III IFNs can also induce mitogen-activated protein kinase (MAPK) signaling⁴⁹.

While the type I IFN receptor (composed of IFNAR1/2 subunits) is ubiquitously expressed, that of IFNLR is not well documented in immune cells. To better understand the mechanism of action of type III IFN and its positive impact on clinical outcome, here we investigate the effects of IFN-III on pDCs compared to other DC subsets. We show that tumor-associated pDCs still express the highest level of IFNLR1, and that these immune cell subsets are the most responsive to IFN-III. IFN-III strongly upregulates TLR7 on pDCs and enhances pathway involved in IFN-I production. More importantly, we observe that IFN-III counteracts the inhibitory effect of TGF- β and PGE2. Our results should foster the development of new immunotherapies enhancing immunostimulatory functions of pDCs.

Results

In contrast to cDCs, pDCs strongly respond to IFN-III

To identify the main immune cells targeted by IFN-III, we first investigated the expression of *IFNLR1* and *IL-10R β* , the two chains of IFNLR, by looking at public RNA sequencing data from the Human Cell Atlas. pDCs displayed the highest RNA level of *IFNLR1* (Fig. 1A), and were the third immune cell population with the highest mRNA level of *IL-10R β* (Fig. 1B). We noted that B cells and cDC1s also expressed a small amount of *IFNLR1* mRNA. In order to better decipher the expression of *IFNLR1* and *IL-10R β* in DC subsets, we FACS-sorted the two conventional DC populations (cDC1s and cDC2s) and pDCs from normal blood and performed RNA sequencing. As shown in Fig. 1C, we observed a very high expression of *IFNLR1* mRNA in pDCs and negligible or very low level in others blood DC, whereas *IL-10R β* was found in the three DC populations albeit at higher levels in pDCs. We then evaluated STAT1 phosphorylation (pSTAT1) in response to IFN-I or IFN-III by flow cytometry in peripheral blood cDCs and other mononuclear cells (PBMCs) (Supplementary Fig. 1A). pDCs were the only blood cells to display a strong increase in pSTAT1 following IFN-III stimulation, which was as strong as the one induced upon IFN-I stimulation (Fig. 1D–E), as previously described^{21–23}. Of note, a slight increase in pSTAT1 on B cells was also observed²⁴ (Supplementary Fig. 1C). Except for pDCs and B cells, neither cDCs, T cells nor NK cells responded to IFN-III (Fig. 1D–E and Supplementary Fig. 1B–C). Thus, pDCs from PBMCs are the immune cells that responded the strongest to IFN-III and the only DC subset sensitive to IFN-III stimulation.

IFN-III increases the survival and expression of activation markers, PD-L1 and ICOS-L on pDCs

Because of the strong response IFN-III induced in pDCs, we evaluated whether it also impacted their phenotype. We thus purified pDCs from

PBMCs and incubated them 24 h with IFN-III or IL-3, which is a classically used survival cytokine for pDCs. We observed that similarly to IL-3, IFN-III significantly increased pDC viability after 24 h of culture, reaching 73.9% against 42.6% in the control condition as previously described by others²¹ (Supplementary Fig. 2A). In addition, IFN-III activated pDCs as observed by the low upregulation of HLA-DR, CD80 and CD86 (Fig. 2A). CD123 is also upregulated by IFN-III as reported previously²¹ suggesting that this cytokine may also modulate pDC sensitivity to a subsequent IL-3 stimulation. Interestingly, the immunoregulatory molecules PD-L1 and ICOS-L were both upregulated after IFN-III stimulation, with around 66.4% and 48.9% of pDCs expressing ICOS-L or PD-L1, respectively (Fig. 2B–D). These results highlight the potential immunomodulatory role of pDCs once stimulated with IFN-III.

IFN-III induces pathways involved in IFN-I production and several main components of TLR7 signaling

To gain further insights into the effects of IFN-III on pDCs, we performed RNA-sequencing on pDCs isolated from PBMCs stimulated with or without IFN-III. After conducting a kinetics experiment, we selected 12 h as the optimal time for the highest ISG expression in response to type III IFN (Supplementary Fig. 2B). We observed that IFN-III did not affect *IFNLR1* and *IL10RB* RNA expression (Supplementary Fig. 3A). Principal component analysis (PCA) on our dataset revealed that IFN-III stimulation was accountable for 45% of the variability between our samples (Fig. 3A). A gene expression analysis showed that IFN-III had an important effect on pDCs, as 1,489 differentially expressed genes (DEGs) were upregulated, and 888 were downregulated when comparing IFN-III-stimulated pDCs *vs* non-stimulated pDCs (Fig. 3B). The upregulation of *CD274* (PD-L1) was observed among DEGs, supporting our previous observation at the protein level (Fig. 2E). Other genes such as *APOL6*, *IFIT2*, *SOC1* involved in JAK/STAT pathways were also highlighted (Fig. 3B).

NLCRS5, the gene with the strongest adjusted *p*-value, involved in the transcriptional regulation of MHC-I was also upregulated (Fig. 3B and Supplementary Fig. 3A). Based on a Gene Set Enrichment Analysis (GSEA), the hallmark gene set with the most important normalized enrichment score was the interferon gamma response (Fig. 3C). In addition, interferon alpha response was the hallmark displaying the highest percentage of enriched genes. Of note, those 2 hallmarks shared almost half of their enriched genes (Supplementary Fig. 2D). Interestingly, the PI3K-AKT-mTOR, the mTORC1 signaling, and protein secretion were hallmarks enriched in IFN-III-stimulated pDCs (Fig. 3C), three pathways involved in type-I IFN secretion^{25,26}. Moreover, our RNAseq analysis showed upregulation of: i) several main components of the TLR7 signaling pathway such as *TLR7* and *IRF7*, ii) UNC93B1 or AP3S1 genes promoting TLR trafficking^{27,28}, iii) HSP90B1 TLR protein chaperone²⁹, iv) PTPN22³⁰, SLC3A2³¹, PI3KAP1³², RSAD2, SCARB2³³, SLC15A4³⁴ or PLSCR1³⁵ described to directly regulate TLR activation. (Supplementary Fig. 2C). Altogether these results suggest that IFN-III stimulation primes pDCs to better respond to TLR in particular TLR7 ligands and to produce a stronger IFN-I response.

IFN-III pre-treatment sensitizes pDCs to low doses of a TLR7 agonist

After demonstrating the priming effect of IFN-III on pDCs, we sought to investigate their enhanced responsiveness to a TLR7 agonist. We initially observed that increased TLR7 mRNA expression (Fig. 4A) was associated with an increased expression of TLR7 at the protein level by flow cytometry (*p*-value = 0.0312) (Fig. 4B, C). Compared to TLR7, none of the other TLRs were significantly affected by IFN-III treatment including TLR1, TLR6 and TLR4, albeit cytosolic pattern recognition receptors RIG-I and MDA5, and CGAS, contributing to antiviral responses were increased (Supplementary Fig. 3A). Of note, TLR9 was

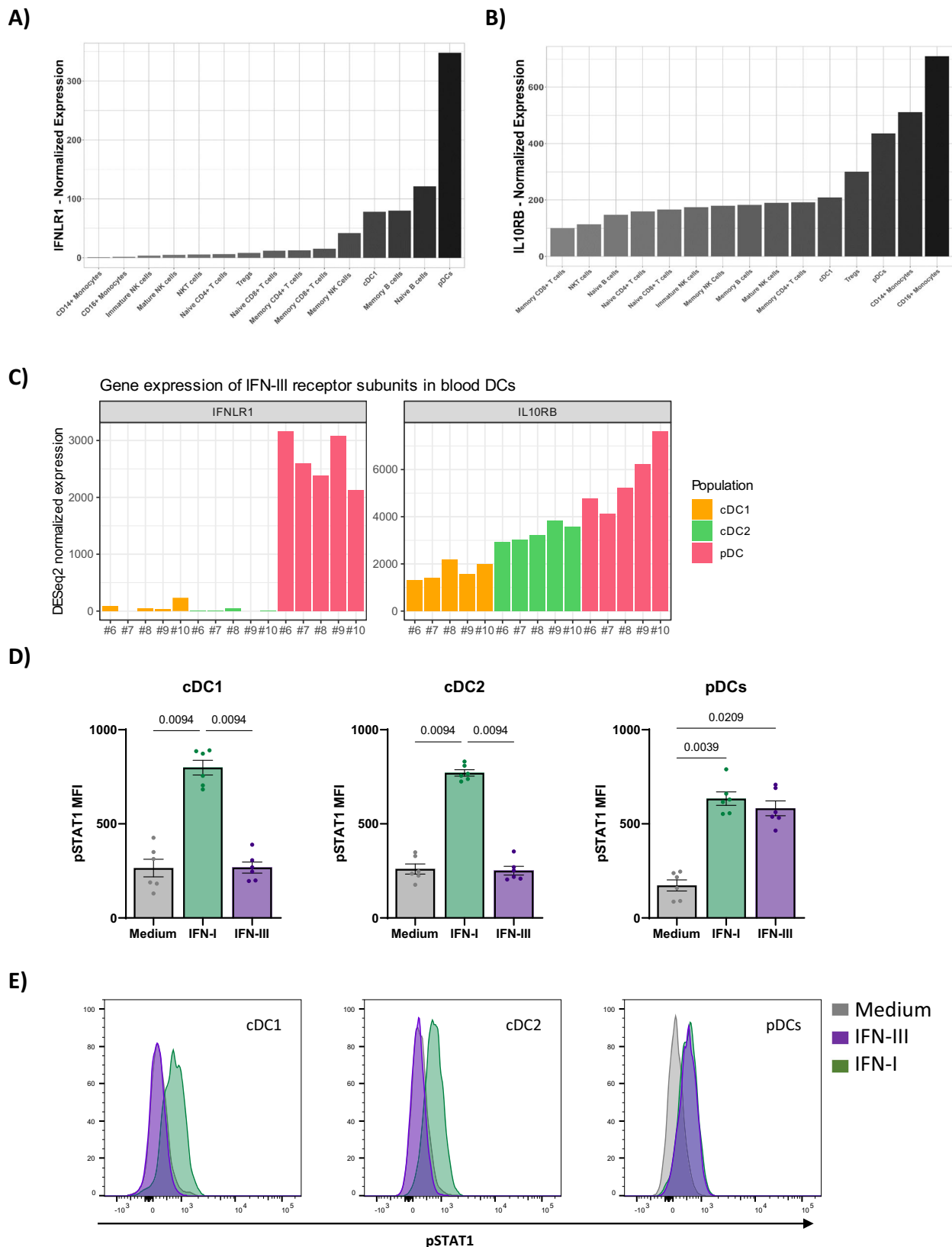


Fig. 1 | pDCs are the only dendritic cells that respond to IFN-III in blood.

A, B Normalized counts were retrieved from public data available from the Human Cell Atlas (HCA) to assess receptor expression of healthy peripheral blood mononuclear cells (PBMCs). **A** IFNL1 expression or **(B)** IL-10R β expression. **C** Blood cDC1s, cDC2s, and pDCs were sorted from 5 blood PBMCs (#6, #7, #8, #9 and #10), RNA was then sequenced to retrieve the normalized counts of IL-28R α and IL-10R β

genes. **D** pSTAT1 levels were measured in cDC1s, cDC2s and pDCs by flow cytometry after 45 min stimulation with 100 ng/mL IFN- λ 1 (purple) or 1000 U/mL IFN- β (green) ($n = 6$ independent donors). Mean values \pm s.e.m are shown. Statistical significance was determined using the two-sided Friedman test on the mean fluorescent intensity (MFI). Source data are provided as a Source Data file. **E** FACS analysis of pSTAT1 level from a representative donor.

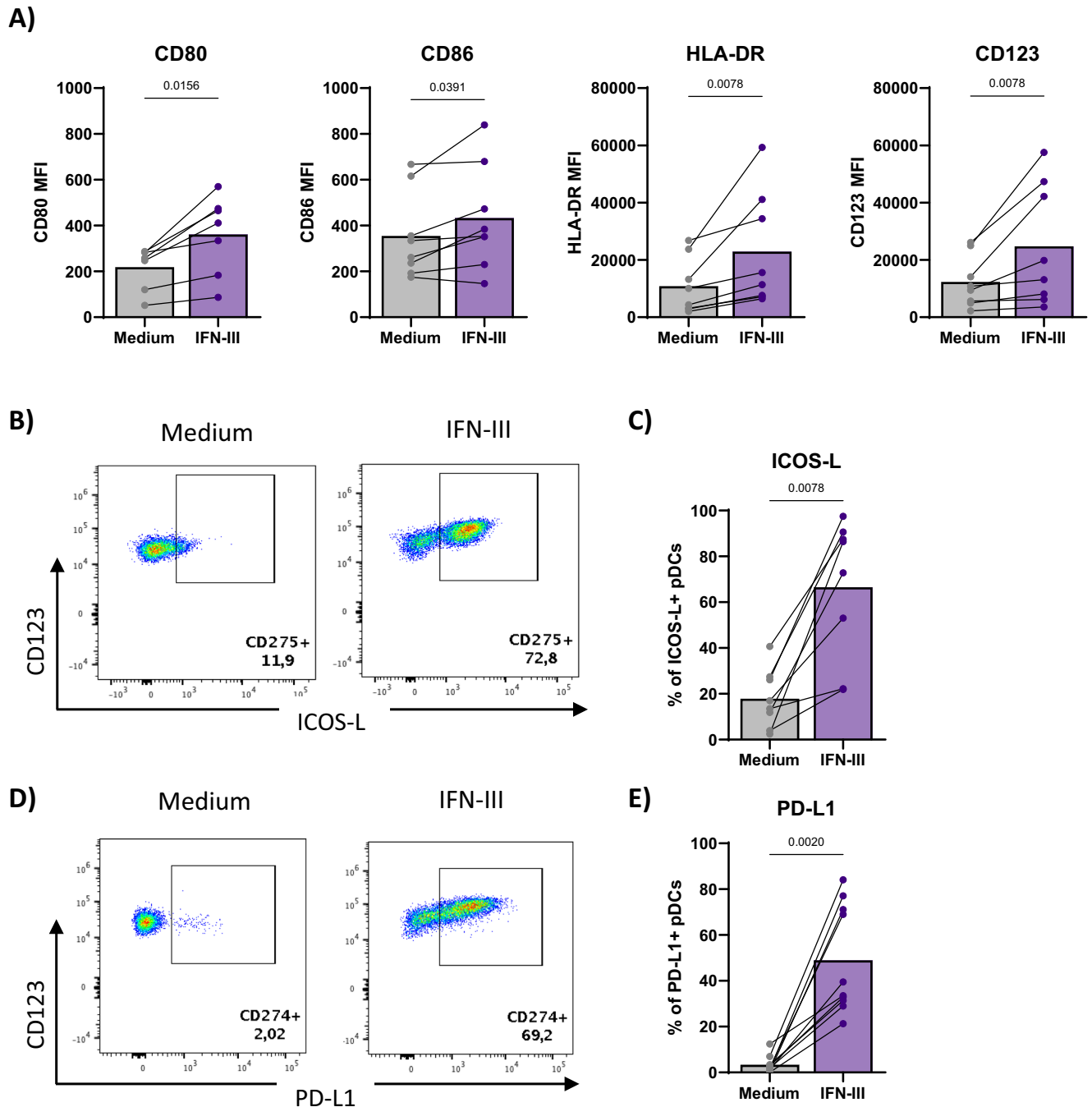


Fig. 2 | Increased expression of activation markers PD-L1 and ICOS-L on pDCs stimulated by IFN-III. **A–E** pDCs were treated 24 h at 37 °C with (purple) or without (gray) 100 ng/mL of IFN- λ 1 (without IL-3). Cells were stained and protein expression was assessed by flow cytometry ($n = 8$ independent donors). Source data are provided as a Source Data file. **A** Quantification of the mean fluorescence intensity (MFI) of the activation markers CD86, CD80, HLA-DR, CD123. **B** pDCs expressing

ICOS-L from a representative healthy donor. **C** Percentage of pDCs expressing ICOS-L at their surface ($n = 8$ independent donors). Source data are provided as a Source Data file. **D** pDCs expressing PD-L1 from a representative healthy donor. **E** Percentage of pDCs expressing PD-L1 at their surface ($n = 10$ independent donors). Source data are provided as a Source Data file. Statistical significance was determined using a two-sided Wilcoxon test.

not upregulated by IFN-III and this was confirmed by flow cytometry (Supplementary Fig. 3B–C).

We then investigated if IFN-III pre-treatment on pDCs would enhance their responsiveness to a TLR7 ligand such as Imiquimod (IMQ). Following a dose response analysis, we selected 50 ng/mL as a suboptimal dose of IMQ for pDC activation and IFN- α secretion (Supplementary Figs. 4A–C). No difference in pDC activation markers was observed at the optimal concentration of IMQ (250 ng/mL), when comparing IFN-III-stimulated pDCs *vs* unstimulated pDCs (Fig. 4D–F).

In contrast, only IFN-III-pre-treated pDCs responded to a suboptimal concentration of IMQ, as evidenced by their upregulation of PD-L1, ICOS-L and HLA-DR expression (Fig. 4D–F). When analyzing the capacity of pDCs to produce IFN- α , we observed a strong enhancement of IFN- α secretion at both suboptimal and optimal doses of IMQ (2146- and 26.4- fold increase respectively) when pDCs were pre-treated with IFN-III compared to untreated pDCs (Fig. 4G).

Altogether these results demonstrate that IFN-III primes pDCs for a stronger response to a TLR7 ligand.

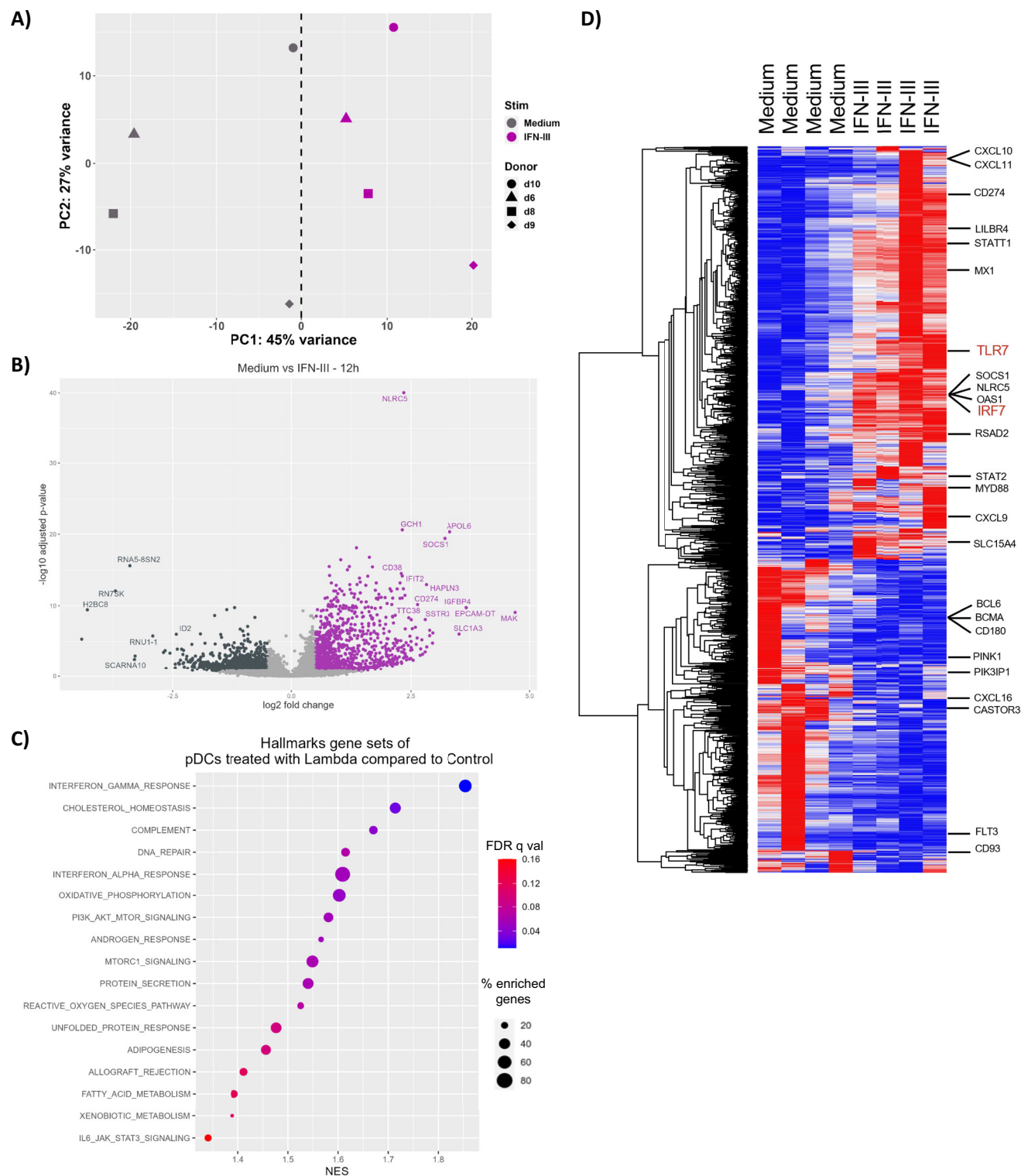


Fig. 3 | IFN-III induces TLR7 and pathways involved in IFN-I production. RNA sequencing was performed on purified pDCs treated with or without 100 ng/mL IFN- λ I for 12 h at 37 °C ($n = 4$ healthy donors; without IL-3). **A** PCA of the normalized RNAseq transcripts per million (TPM) of purified pDCs treated or not with IFN-III. **B** Volcano plot representation of differentially expressed genes (DEGs) in IFN-III-treated pDCs versus untreated pDCs. The x-axis shows \log_2 fold changes in expression and the y-axis the $-\log_{10}$ adjusted p -value of each DEG obtained with DESeq2 R package using the Wald test. p -values obtained by the Wald test are

corrected for multiple testing using the Benjamini and Hochberg method. **C** GSEA Hallmark analysis showing enriched gene sets. The x-axis represents the normalized enriched score indicating the hallmark enrichment in IFN-III-treated pDCs versus untreated pDCs. FDR q values are represented in a gradient of blue-to-red and the size of each dot represents the percentage of genes enriched for each hallmark. **D** Heatmap of z-scores of RNAseq expression using all 3129 DEGs. Each column corresponds to a sample and each row corresponds to a specific gene.

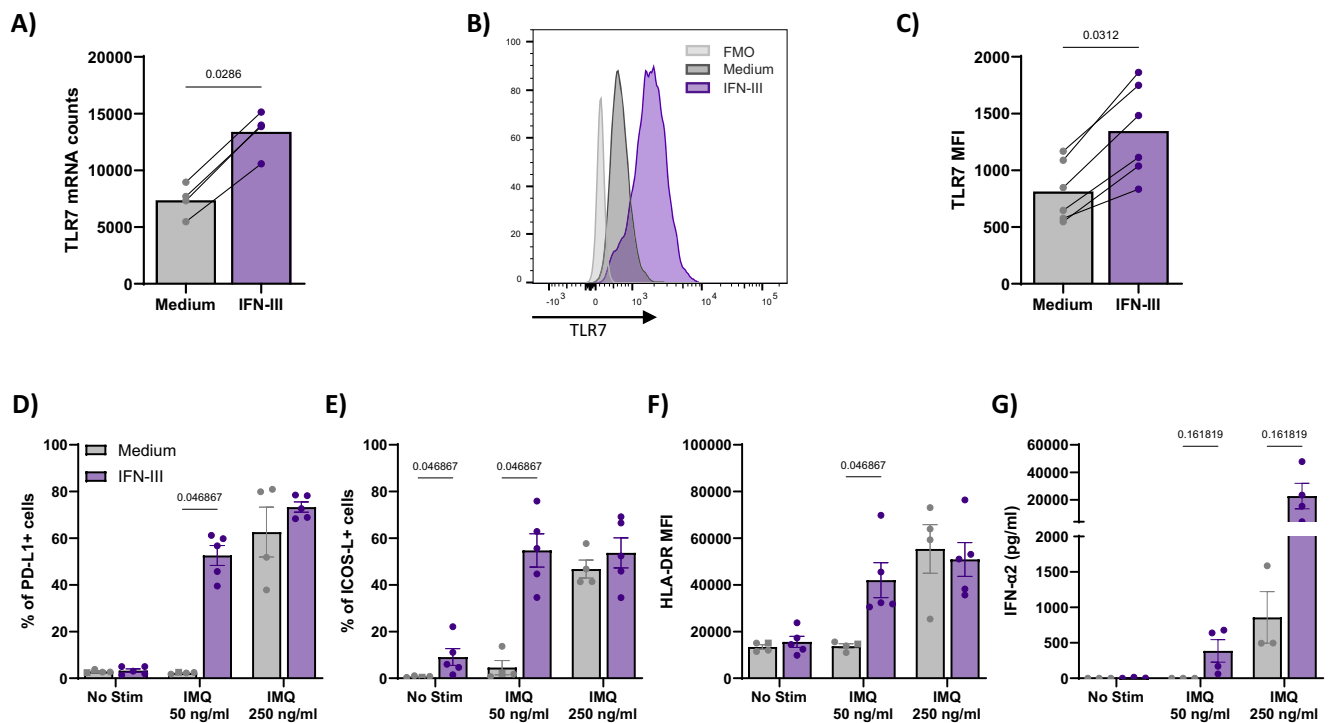


Fig. 4 | IFN-III pre-treatment sensitizes pDCs to low doses of Imiquimod. **A** TLR7 normalized counts from RNA sequencing of pDCs treated with (purple) or without (gray) 100 ng/mL IFN- λ 1 for 12 h ($n = 4$ independent donors). Statistical significance was addressed with a two-sided Wilcoxon test. Source data are provided as a Source Data file. **B**, **C** TLR7 protein expression was evaluated by flow cytometry on purified pDCs treated (purple) or not (gray) with 100 ng/mL IFN- λ 1 for 18 h. Source data are provided as a Source Data file. **B** TLR7 expression from a representative donor **C** Bar plot with individual values of TLR7 expression from healthy donors ($n = 6$ independent donors). Statistical significance was addressed with a two-sided Wilcoxon test. **D** PD-L1-positive, **E** ICOS-L-positive pDCs and **F** HLA-DR MFI were quantified by flow cytometry after different combinations of treatment with or

without IFN- λ 1 (100 ng/mL) for 18 h followed by 50 or 250 ng/mL Imiquimod (IMQ) or no Imiquimod (“No stim”) for 24 h. **D–F** Without IFN- λ 1 pre-treatment, cells were kept at 4 °C (Medium) before IMQ stimulation ($n =$ minimum 3 independent donors). **G** IFN- α 2a was quantified by electrochemiluminescence multiplex assay (MSD) in the supernatants of pDCs cultured after different combinations of pre-treatment for 18 h followed by 250 ng/mL or 50 ng/mL of Imiquimod, or no Imiquimod (“No stim”) for 24 h. All culture conditions were performed without IL-3 on minimum $n = 3$ independent donors. Mean values \pm s.e.m are shown. Source data are provided as a Source Data file. Statistical significance was determined using a two-sided Mann-Whitney test.

IFN-III-stimulated pDCs acquire an IFN-I secretory phenotype upon TLR-7 stimulation

Knowing that IFN-III primes pDCs for TLR7 activation, we wanted to evaluate whether a different survival factor may drive a different pDC state. To address this question, we activated pDCs with a high dose of IMQ (250 ng/mL) and with either IFN-III which is associated with a more innate environment or another survival factor, here IL-3, which mimics a more immune adaptative contexture as T cells are the major source of IL-3³⁶.

As shown in Fig. 5A–C, after IMQ stimulation, 73.7% of IFN-III-pre-treated pDCs were PD-L1⁺ CD80^{neg} which, as described by Alculumbre et al., are IFN-type I-secreting pDCs (named P1)³⁷. In contrast, within the IL-3-pre-treated pDCs, only 14.6% of cells belong to the P1 population (Fig. 5C). When pDCs were pre-treated with both IFN-III and IL-3, the P1 subpopulation reached 24.4%. In contrast, P3 subpopulations characterized as PD-L1^{neg} CD80⁺ and associated with adaptive immunity, as they can activate T cells, were absent in IFN-III pre-treated pDCs but present in 42.9% of IL-3-pre-treated pDCs. The polarization of pDCs towards a subpopulation specialized in IFN- α secretion was confirmed by the high amount of IFN- α detected in IFN-III-pre-treated pDC supernatants (24.5 ng/mL against 7.2 ng/mL with IL-3 pre-treatment in response to IMQ) (Fig. 5D) and was also observed at a sub-optimal dose of IMQ (Supplementary Figs. 5A–F). Of note, the priming of pDCs with both IL-3 and IFN-III resulted in a mixed phenotype with P1 and P3 cells, named P2 which exists only in this culture condition (Fig. 5A, B). Similar IFN- α secretion levels were observed in IFN-III and IFN-III + IL-3 conditions. This indicates that IFN- α -producing cells may be included i) in

the P2 population or ii) in the small P1 population observed in IL-3 + IFN-III.

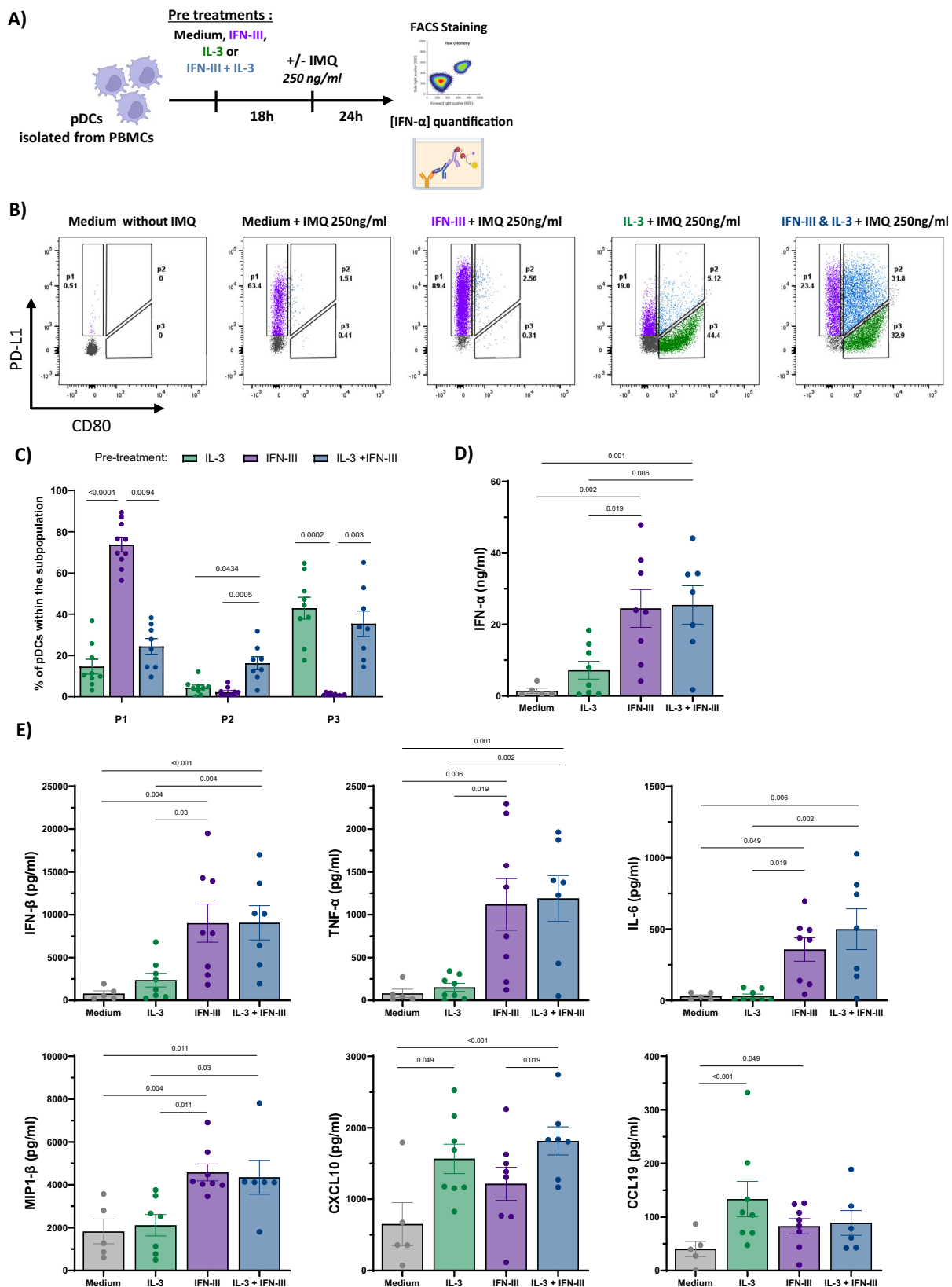
IL-3 alone also impacted the pDC phenotype after 42 h, as evidence by the increase in activation markers (CD80, 86, PD-L1, HLA-DR and ICOSL) to similar levels to those observed with the suboptimal dose of IMQ (Supplementary Figs. 5 C–D). We observed that PD-L1, CD80 and ICOSL expression induced by IFN-III without IMQ (reported in Fig. 2 after 24 h treatment) was lost at 42 h (Supplementary Fig. 5C), suggesting a transient activation stage without a direct TLR stimulation.

In response to IMQ, IFN-III-pre-treated pDCs were also shown to secrete a high dose of IFN- β , along with innate and inflammatory cytokines MIP1- β , IL-6, and TFN- α compared to IL-3-pre-treated pDCs (Fig. 5E). Conversely, CCL19 and CXCL10, two cytokines implicated in T cell recruitment, were increased when pDCs were pre-treated with IL-3, which is consistent with a specialization towards an APC function and T cell activation (Fig. 5E).

In conclusion, the response of pDCs to a TLR stimulation depends on the immune context potentially resulting in a more inflammatory response or in a T cell recruitment environment.

cDC1s and pDCs interact through type I and III IFNs axis and are in close contact or in the same discrete area of the TME

We previously demonstrated that the very large majority of cells able to produce IFN-III in the breast TME are cDC1s¹⁸. We hypothesized that pDCs localized close enough to cDC1s that secrete IFN-III may acquire an IFN-producing phenotype. To determine pDC and cDC1 localization



in the TME, we performed multiplex-immunofluorescence (mIF) staining on 10 Triple Negative Breast Cancer (TNBC). We observed numerous cDC1s (XCR1+) co-localizing with pDCs (BDCA2+) (Fig. 6A). By performing image segmentation analysis with Inform software and cell-cell distance calculations with bioinformatics tools, we quantified close contacts between pDCs and cDC1s (defined by a

distance from the center of two nuclei $< 15 \mu\text{m}$). 9% of cDC1s were in close contact with at least one pDC (Fig. 6B–C). However, as IFN-III is a cytokine, immune cells affected by the cytokine may not be in direct contact to benefit from its action. Hence, we observed that 4.2, 2.3, and 0.5 pDCs on average are within a 100 μm , 70 μm and 30 μm radius of the cDC1s, respectively (Fig. 6D). These results demonstrate that

Fig. 5 | IFN-III-stimulated pDCs acquire an IFN-I secretion phenotype upon TLR7 stimulation and favors the secretion of numerous cytokines and chemokines. **A** Schematic representation of the experimental protocol. **B–C** Percentage analysis of pDC subpopulations P1, P2, and P3 according to their expression of PD-L1 and CD80 after pre-treatment and IMQ exposure assessed by flow cytometry. **B** One representative FACS plots of the different experimental conditions **C** P1, P2, and P3 distribution following different pre-treatments and IMQ activation ($n = 10$ independent donors). Mean values \pm s.e.m are shown. Source data

are provided as a Source Data file. **D** IFN- α 2a and **E** IFN- β , TNF- α , IL-6, MIP1- β , CXCL10, CCL19 were quantified by multiplex assay in the supernatants of pDCs pre-treated with IFN-III or IL-3 for 18 h before being stimulated 24 h with 250 ng/mL IMQ ($n = 7$ independent donors). Without pre-treatment, cells were kept at 4 °C (Medium) before IMQ stimulation. Statistical significance was determined using a two-sided Kruskal-Wallis test (**C**) and two-sided Friedman test (**D–E**). Each point represents a separate donor (**C–E**). Mean values \pm s.e.m are shown (**D, E**). Source data are provided as a Source Data file.

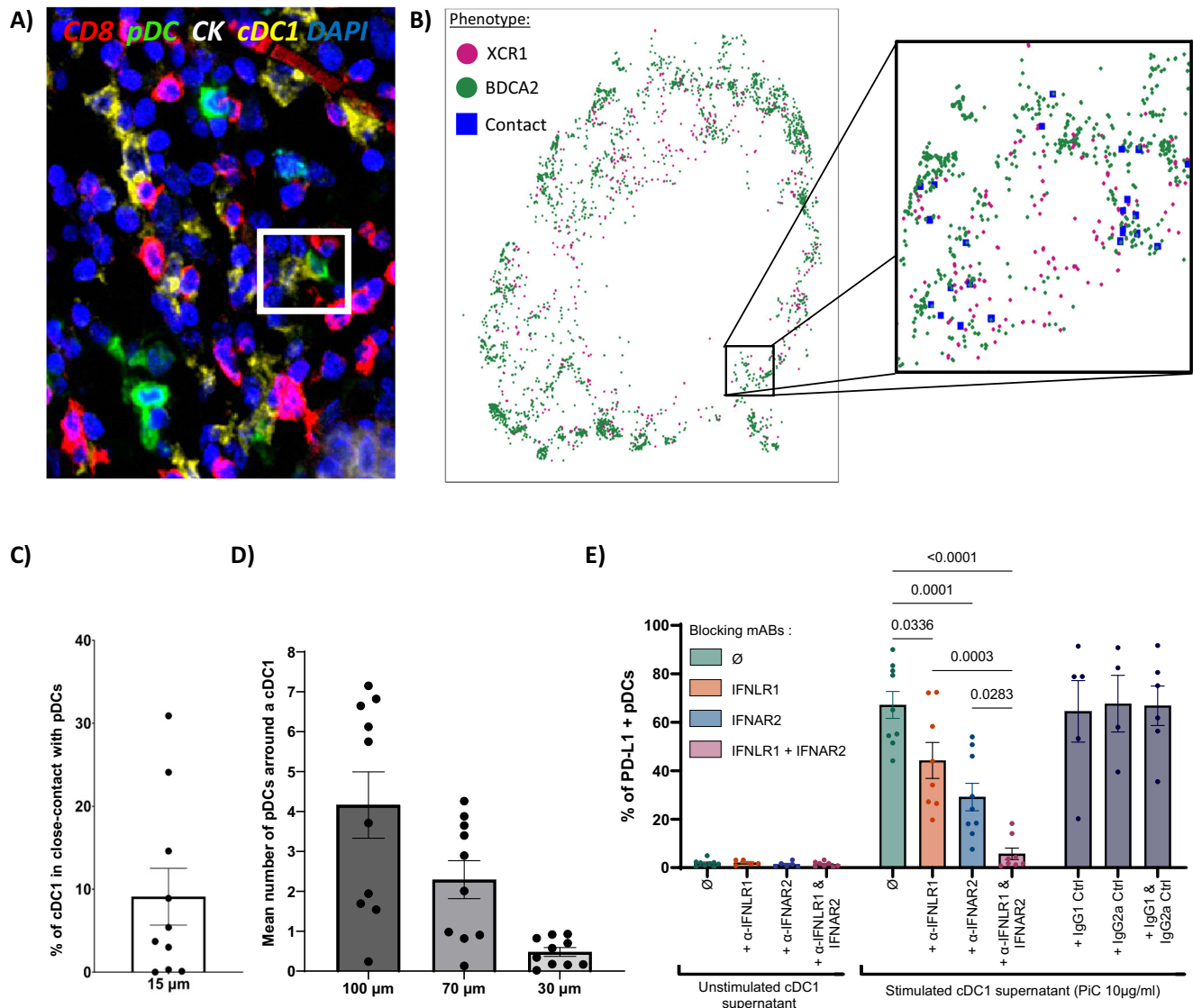


Fig. 6 | cDC1s and pDCs interact through type I and III IFNs axis and are in close contact or in the same discrete area of the TME. **A** Visualization of CD8 + T cells, pDCs, cancer cells, cDC1s, respectively by CD8 (red), BDCA2 (green), cytokeratin (white), XCR1 (yellow) using multiplex IF (mIF). Nuclei were stained with DAPI. The white square focuses on a close contact between a cDC1 with a pDC observed in 7 out of 10 triple negative breast tumors. Magnitude $\times 50$ **(B)** 2D projection of cDC1s (purple) and pDCs (green) present in a whole tumor slide of triple negative breast cancer. Blue squares represent a close contact between cDC1 and pDC (distance from nuclei center $< 15 \mu$ m). **C** Percentage of XCR1 + cDC1 in close-contact with pDCs in 10 triple negative breast tumors. Mean values \pm s.e.m are shown. **D** The

number of pDCs present in each cDC1 area (radius = 100, 70, 30 μ m) was calculated in the 10 whole tumor slides. Mean values \pm s.e.m are shown. Source data are provided as a Source Data file. **E** Percentage of PD-L1 positive pDCs after 24 h with supernatants of FACS sorted human in-vitro generated cDC1 stimulated with 10 μ g/ml Poly(I:C) 24 h. Before stimulation, pDCs were incubated 1 h with [IFNLR1] or / and [IFNAR2] blocking antibodies (5 μ g/ml). [Mouse IgG1] & [mouse IgG2a] (5 μ g/ml) were used as isotype controls. Each point represents a separate donor and there is no technical replicate. Mean values \pm s.e.m are shown (minimum $n = 4$ independent donors).

tumor-associated (TA)-pDCs are often located near a TA-cDC1s and may benefit from their IFN-III secretion, since IL-3 is rarely found in the supernatant of tumors (except in 2 breast tumors over 65 and 1 ovarian tumors over 13; see Suppl. Source Data and Supplementary Fig. 6).

To further validate a potential cross-talk between cDC1s and pDCs, we stimulated pDCs in vitro with poly:I:C-activated cDC1 supernatant with or without IFNLR1 blocking mAb. This mAb has been validated in pDC using exogenous recombinant IFN-III

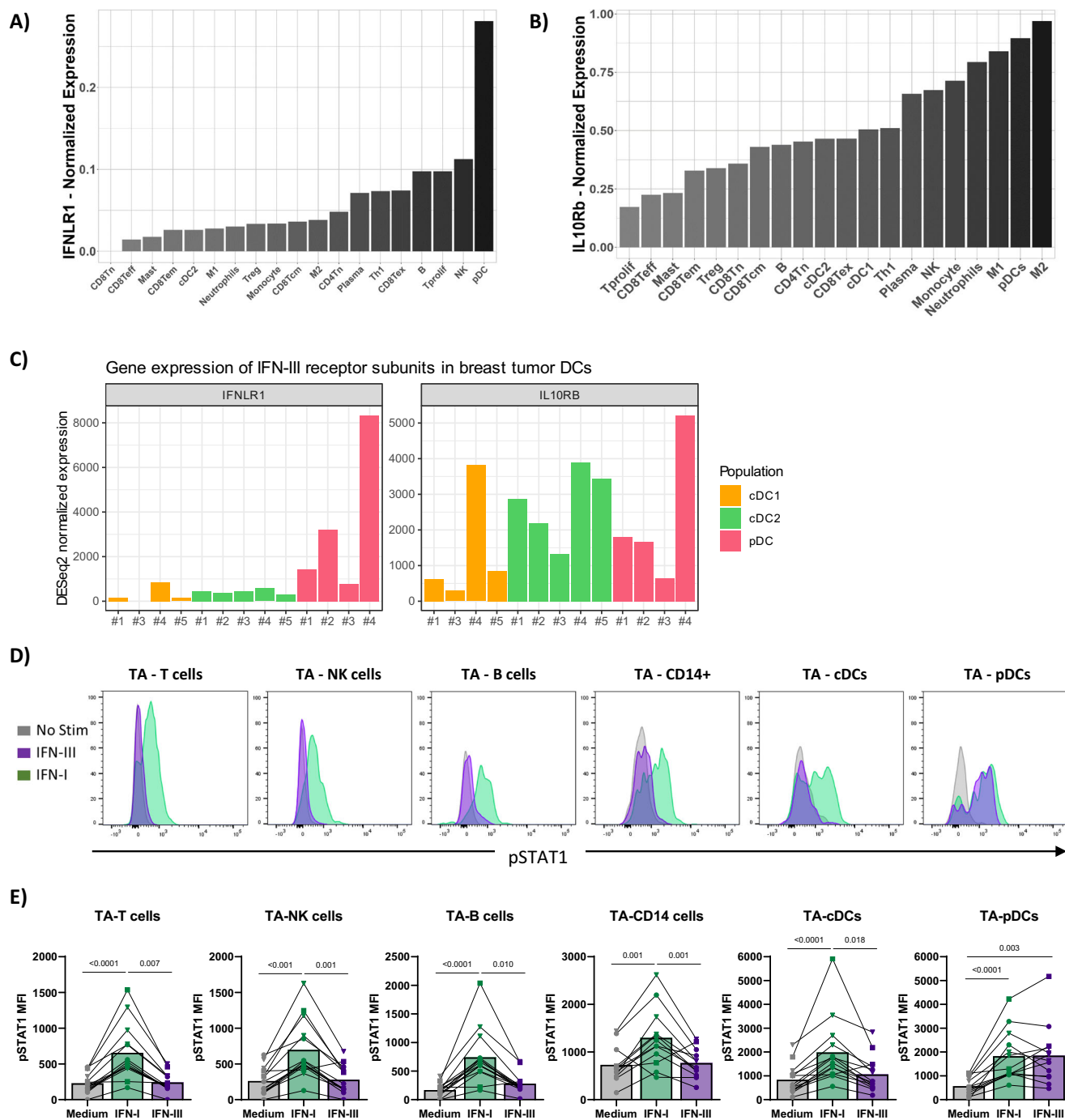


Fig. 7 | Tumor-associated pDCs strongly respond to IFN-III. **A, B** Normalized counts were retrieved from public data available on the Tumor Immune Single-cell Hub (TISCH) to assess receptor expression of human tumor-infiltrating immune cells. **A** IFNL1 expression or **(B)** IL10RB expression. **C** Tumor-associated cDC1s, cDC2s, and pDCs were sorted from 4 or 5 breast tumors (patients #1, #2, #3, #4 and #5), RNA was then sequenced to retrieve the normalized counts of IL-28R α and IL-10R β genes. **D, E** Tumor-associated immune cells were cultured with IFN-I (green)

or IFN- λ I (purple) for 45 min at 37 °C and pSTAT1 was analyzed. **D** Representative histograms of pSTAT1 in sorted immune cells from an ovarian tumor sample.

E pSTAT1 from breast tumor ($n = 2$: square), ovarian tumors ($n = 4$: triangle), lung tumors ($n = 7$: circle) infiltrating cells. Source data are provided as a Source Data file. Statistical significance was determined using a two-sided Friedman test on mean fluorescence intensity (MFI) values.

(Supplementary Fig. 7A). As shown in Fig. 6E, blockade of either type I or type III IFN receptor only partially reduced PD-L1 expression by activated pDCs, whereas inhibition of both receptors completely abolished PDL1 upregulation. Increased expression of other markers such as ICOS-L, HLA-DR, CD123 and CD86 were not affected by IFN blockade (Supplementary Fig. 7B). This suggests a role for other cytokines secreted by cDC1s in their cross-talk with surrounding pDCs such as TNF- α . Nevertheless, while we showed that blood pDCs

responded to IFN-III (Figs. 1–5), the capacity of TA-pDCs to be responsive to IFN-type III needs to be demonstrated.

Tumor-associated pDCs strongly respond to IFN-III

In order to decipher if TA-pDCs respond to IFN-III, we first used available public transcriptomic data to analyze their expression of *IFNL1* and *IL-10R β* chains (Fig. 7A–B). These findings revealed that TA-pDCs exhibit the highest mRNA expression of *IFNL1* among all

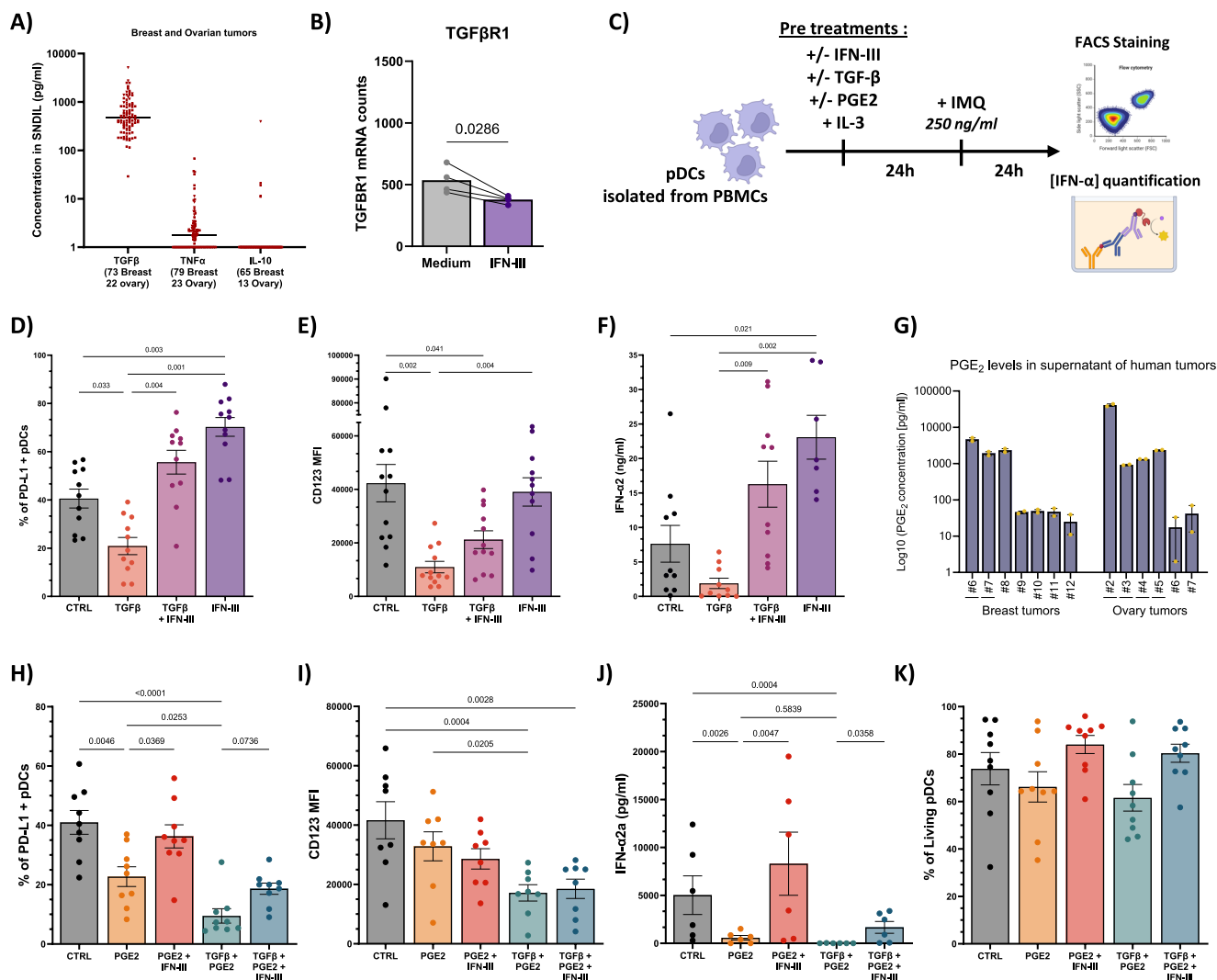


Fig. 8 | IFN-III prevents pDCs inhibition induced by exogenous immunosuppressive cytokines. **A** TGF- β , TNF- α and IL-10 concentrations were quantified using a multiplex immune assay kit in supernatants of primary dilacerated breast (square) and ovarian (triangle) tumors (SN-DIL). **B** TGF- β -RI normalized counts from RNA sequencing of pDCs treated with (purple) or without (gray) 100 ng/mL IFN- λ 1 for 12 h ($n = 4$ independent donors). Statistical significance was addressed with a two-sided Wilcoxon test. **C** Schematic diagram of the experimental procedure using [TGF- β] = 2 ng/mL, [PGE2] = 10 μ M, [IFN- λ 1] = 100 ng/mL. All conditions were in the presence of 20 ng/mL IL-3 to preserve good pDC viability under all conditions. **D–H** Percentage of PD-L1 positive pDCs and CD123 MFI on pDCs (**E–I**) after 48 h treatment at 37 °C in different conditions with 250 ng/mL IMQ. Mean values \pm s.e.m

are shown. Source data are provided as a Source Data file. Minimum $n = 8$ independent donors. **G** PGE2 was quantified using PGE2 Elisa assay kit in the supernatants of primary dilacerated breast ($n = 7$) and ovarian tumors ($n = 6$). **F, J** Quantification of IFN- α 2 (pg/mL or ng/mL) secreted by pDCs after 48 h treatment at 37 °C in different conditions with 250 ng/mL IMQ. Mean values \pm s.e.m are shown. Source data are provided as a Source Data file. Minimum $n = 6$ independent donors. Statistical significance was determined using a two-sided Friedman test. **K** Viability of treated pDC in culture conditions described in panel C. Mean values \pm s.e.m are shown ($n = 9$ independent donors). Source data are provided as a Source Data file.

infiltrating immune cells. TA-pDCs also expressed a high level of *IL-10RB*, though the highest expression was reached by M2 macrophages (Fig. 7B). However, not all DC subsets were present in the public transcriptomic data. Thus, we FACS-sorted cDC1s, cDC2s, and pDCs from breast tumors and performed bulk RNA sequencing (Fig. 7C). Within tumor-associated DC (TA-DCs) subsets, pDCs remained the subset with the highest expression of *IFNL1* (Fig. 7C). Regarding *IL-10RB*, its expression appeared robust in cDC2s, and pDCs, while showing a weaker level in cDC1s.

To confirm that the response of TA-pDCs to IFN-III is functional, we processed breast, ovarian, and lung tumors to obtain cell suspensions of TA immune cells and stimulated them with IFN-I or IFN-III. While all immune cells responded to IFN-I, only TA-pDCs responded to IFN-III with variable intensity, as illustrated by the increase in pSTAT1 similar to that induced by IFN-I (Fig. 7D–E). Altogether, we show that in

three tumor types, pDCs are the only immune cell type able to respond to IFN-III.

IFN-III counteracts TGF- β and PGE2 inhibition by enhancing IFN-I production by pDCs upon TLR7 stimulation

Even though TA-pDCs responded to IFN-III, it has been reported that IFN- α production by pDCs is inhibited by TGF- β and TNF- α secreted in the TME^{13,14,38}. Using supernatants from primary dilacerated breast and ovarian tumors (SN-DIL), we detected high level of TGF- β 1 in SN-DILs, whereas no or low levels of TNF- α and IL-10 were observed (Fig. 8A). By further exploring our RNAseq data on pDCs, we found that IFN-III-stimulated pDCs displayed a significant decrease in *TGFB1* expression (Fig. 8B). As IFN-III strongly increases IFN-I production and decreases *TGFB1* expression, we wondered if IFN-III could counteract TGF-beta-mediated inhibition of type I IFN secretion. As shown in Fig. 8C–F, TGF- β

pre-treatment inhibited pDCs, as evidenced by a decrease in PD-L1 expression in response IMQ (20.8% with TGF- β compared to 40.6 % in the control with high dose IMQ). We found no significant inhibitory effect of TGF- β on ICOS-L or HLA-DR expression by pDCs in this condition (IL-3 + IMQ 250 ng/mL; see Supp Figs. 8A–B). Interestingly, IFN-III pre-treatment protected pDCs from TGF- β -mediated inhibition of type I IFN secretion with a high or sub-optimal dose of IMQ (Fig. 8C–F and Supplementary Fig. 8D). Indeed, adding IFN-III to TGF- β in pDC pre-treatment restored PD-L1 expression as the percentage of PD-L1+ pDCs reached 55.6% (Fig. 8D). Furthermore, the expression of the IL-3 receptor CD123 was completely downregulated by TGF- β , suggesting that pDC survival may be impacted in the absence of IFN-III. It can also be noted that IFN-III restores CD123 expression in the presence of TGF- β (Fig. 8E). In addition, IFN-III also restored innate chemokine secretion by pDCs such as MIP1- β , IL-8, CXCL10 and IFN- β , all inhibited by TGF- β (Supplementary Fig. 8E). Importantly, by quantifying IFN- α in the supernatant, we observed that IFN- α production can be restored when pDCs are pre-treated with IFN-III (Fig. 8F). This clearly demonstrates that IFN-III can counteract the TGF- β inhibition of pDCs.

Other immunosuppressive cytokines, such as PGE2 are found in the tumor and it was previously demonstrated that PGE2 also inhibits pDC function^{14,16}. We quantified PGE2 in 13 supernatants from dilacerated breast and ovarian tumors (SN-DIL) and observed a large heterogeneity with some tumors containing high or negligible levels of PGE2 (Fig. 8G). We thus treated pDCs with TGF- β or PGE2 or both. We observed pDC inhibition with PGE2 alone, as expected, and the effect was higher when the two immunosuppressive compounds were combined, with a complete abrogation of pDC IFN- α production (Fig. 8J). The PGE2 effect might also be due to the induction of a slight mortality, which is reversed by IFN-III treatment (Fig. 8K). Finally, and very interestingly, we observed that IFN-III was able to partially reverse the strong inhibitory effect of PGE2 + TGF- β , restoring PD-L1 expression (Fig. 8H) and IFN- α production (Fig. 8J).

IFN-III counteracts the TME- induced inhibition of pDC function

Whereas TGF- β and PGE2 are two main immunosuppressive elements present in tumors which inhibit pDCs, other cytokines may synergize in the TME to inhibit TA-pDC functions. We thus performed the same experiments with supernatants from dilacerated breast and ovarian tumors (SN-DIL) to assess the impact of soluble factors collected directly from fresh tumor samples. For this aim, we selected some SN-DILs containing high levels of TGF- β or PGE2 (Supplementary Fig. 9A). As expected, activation of pDCs by IMQ and their subsequent ability to produce IFN- α and IFN- β were significantly inhibited by the different SN-DILs, reflecting the inhibition of these cells in tumors without strongly affecting their viability (Fig. 9A, B, C and Supplementary Fig. 9B–C). Interestingly, we observed that IFN-III completely prevented breast and ovarian SN-DIL-induced inhibition of pDCs by almost completely restoring their PD-L1 (Fig. 9B) and IFN- α secretion capacity (Fig. 9C).

Then, in order to clearly decipher the role of TGF- β and PGE2 in SN-DILs, we performed similar experiments with TGF- β or PGE2 blockade. As shown in Fig. 9D–E, we observed that TGF- β or PGE2 receptor blockade alone did not totally restore pDC function depending on the SN-DILs used. In contrast, blocking the two pathways completely restored PD-L1 expression on pDCs and their IFN- α production in half of the cases (Fig. 9D–E).

We also quantified IFN- λ 1 and IFN- α in 80 breast and 24 ovarian SN-DILs and detected only 13 breast and 3 ovarian tumors expressing IFN- α 2 at a very low level (mean = 2.73 pg/mL and a max of 30.63 pg/mL in breast tumors; see Supp. Source Data). Nevertheless, we clearly observed a higher amount of IFN- α in IFN- λ 1-containing SN-DILs (Fig. 9F). In contrast, IFN- α was mostly observed on TGF- β low SN-DILs, further suggesting a role in TGF- β to damped the type I-production by pDCs in human tumors (Fig. 9F). Moreover, the TGF- β activation

pathway was enriched in TA-pDCs compared to blood pDCs as well as IFN pathways as observed using GSEA analysis on RNA-seq of purified TA-pDCs (Fig. 9G). This further suggests that pDCs are influenced by these two cytokines in the TME.

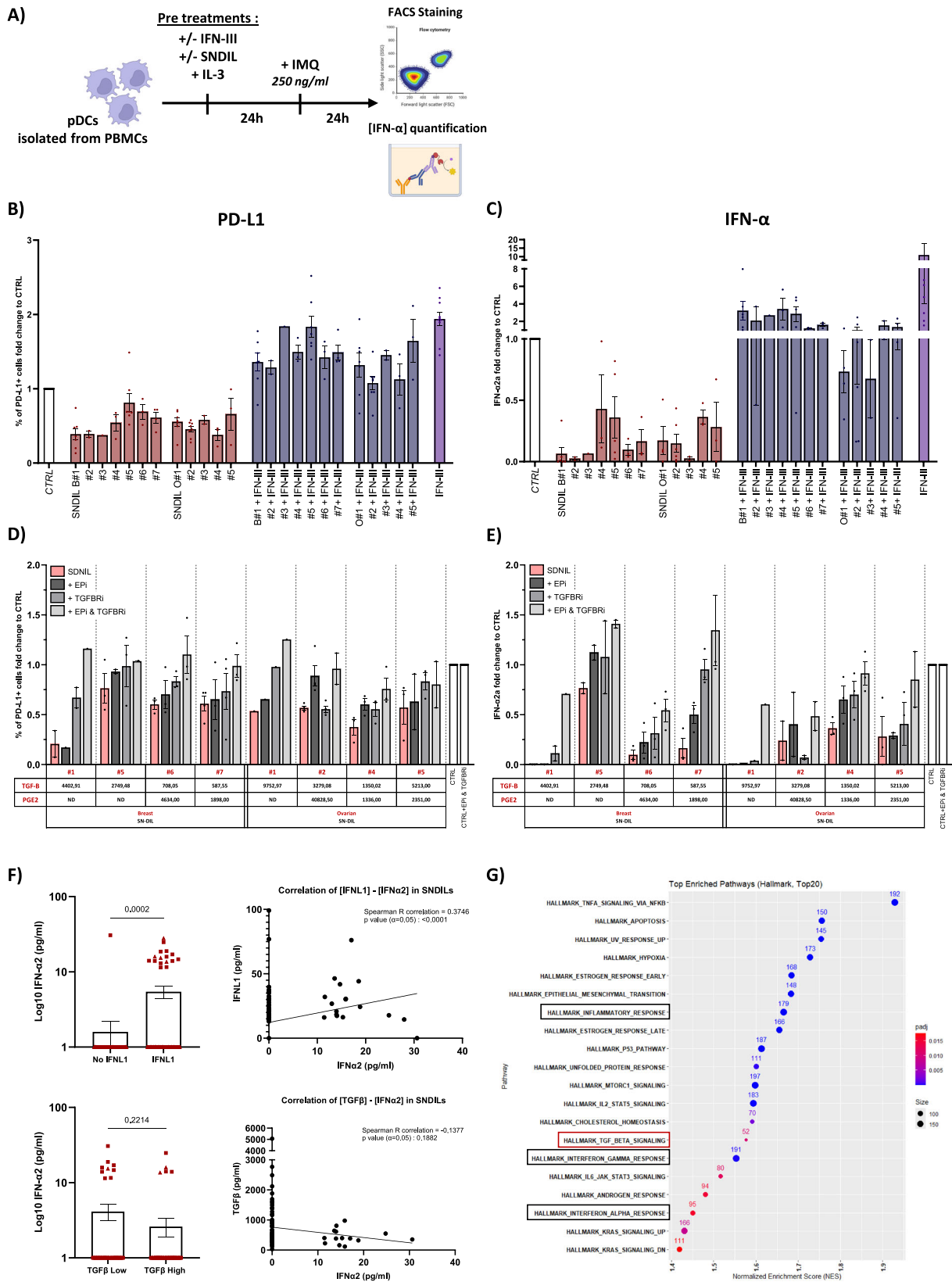
Altogether, these results indicate that IFN-III may restore pDC function in tumors for subsequent activation participating in the anti-tumor immunity.

Discussion

In this paper, we demonstrated for the first time, that TA-pDCs infiltrating breast, lung and ovarian tumors express the highest mRNA levels of *IFNLRI* receptor chain in the tumor microenvironment and are the strongest IFN-III responsive immune cells with activation of the JAK-STAT signaling pathway. We further observed that IFN-III increases pDCs survival, activation and TLR7 expression, enhancing their capacity to respond to a TLR7-ligand. Importantly, IFN-III prevents the inhibition of pDCs induced by the TME soluble milieu or by TGF- β or PGE2, two dominant TME inhibitory cues, and restores their production of IFN- α .

It cannot be excluded that some immune cells may upregulate the IFN-III receptor in response to other signals, making them responsive to IFN-III. In human, in public data of scRNAseq including neutrophils, *IFNLRI* expression was not detected in the neutrophil cluster (data not shown). Nevertheless, it has been reported that human neutrophils can express *IFNLRI* genes after TLR4 stimulation³⁹. Thus, it is possible that in specific pathological situations, immune cells other than pDCs may express the IFN-III receptor. It has also been shown that *IFNLRI* expression increases in HCV-infected human liver and specifically in hepatocytes in response to IFN- α ⁴⁰. *IFNLRI* and CD123 were also shown to be upregulated by IL-3 and IFN-III²², suggesting many amplification loops that may arise when the two cytokines are added simultaneously. Of note, the priming with both IL-3 and IFN-III results in a mixed phenotype with P1 and P3 cells named P2 that exists only in this culture condition. The emergence of this mixed population expressing both activation markers and IFN- α production capacity undoubtedly requires further analysis by scRNAseq in order to identify whether it is a single population supporting the hypothesis of a continuum of pDC differentiation towards an activation state or several pDC subsets, supporting the hypothesis of cell differentiation from distinct precursors³⁷. This may also reflect the pDC evolution in a pathological context⁴¹ where the pDC IFN-I production and T cell activation are performed by the same pDCs, but occur sequentially in time and in different micro-anatomical locations⁴².

As pDCs die rapidly in cell culture, IL-3 is frequently used in vitro^{43,44}. However, the effects of IL-3 on pDCs are not well documented and seem to induce various phenotypic modifications. Indeed, we observed that pDCs activated in the presence of IL-3 are able to upregulate CD80/86 and ICOS-L costimulatory signals, suggesting some APC-related function^{37,43,44}. Furthermore, IL-3-treated pDCs were described to activate and favor IL-4-, IL-5-, and IL-13-producing T cells associated with a Th2 response^{45,46}. OX40L has also been reported to play a role in priming the Th2 response by IL-3-treated pDCs⁴⁷. Nevertheless, we scarcely observed IL-3 in the TME of breast or ovarian tumors, whereas IFN-III protein was largely present¹⁸. Comparatively, we showed that IFN-III favors pDC secretion of cytokines and chemokines triggering an inflammatory response (IL6, TNF- α and MIP1 β). The greater impact of IFN-III than that of IL-3 on the expression of IFN- β , TNF- α or IL-6 may be related to NF κ B activation. In accordance, it was shown by Hosokawa et al.⁴⁸ that an inhibitor of the NF κ B pathway can modulate the production of IP10 in oral epithelial cells after IFN-III treatment. Thus, the cytokine environment in which pDCs encounter a TLR ligand will strongly influence their immune response, demonstrating once again the great plasticity of these cells. Finally, Abbas et al. also described different pDC functions according to different states of activation fluctuating with viral infection (MCMV infection)⁴².



RNAseq data revealed that the PI3K-AKT-mTORC pathway was enriched in IFN-III-treated pDCs. Indeed, the mTORC pathway is essential for IFN- α production in pDCs in response to TLR^{25,26}. The PI3K kinase is necessary for IRF7 nuclear translocation, and mTORC inhibition by the rapamycin completely prevents IFN- α production by pDCs. Of note, this could be a problem in non-targeted therapies that aim at

inhibiting mTORC in cancer cells. Furthermore, oxidative phosphorylation and protein secretion hallmarks enriched in IFN-III stimulated-pDCs also illustrated their priming towards an enhanced secretory ability. Moreover, consistent with this IFN- α -producing phenotype, our RNAseq analysis showed upregulation of many genes involved in TLR trafficking and signaling. However, it is important to highlight that

Fig. 9 | IFN-III prevents inhibition of pDCs induced by TME immunosuppressive cytokines such as TGF- β and PGE2. **A** Schematic diagram of the experimental procedure. All conditions were in the presence of 20 ng/mL IL-3 to preserve good pDC viability under all conditions and stimulated with high dose of IMQ (250 ng/mL). Mean values \pm s.e.m are shown. Source data are provided as a Source Data file. **B** Percentage of PD-L1 positive pDCs, **C** Quantification of IFN- α 2 (ng/mL) secreted by pDCs in different conditions. Mean values \pm s.e.m are shown. Source data are provided as a Source Data file. **D** Percentage of PD-L1 positive pDCs and **(E)** Quantification of IFN- α 2 (ng/mL) secreted by pDCs in the different conditions. Before pre-treatments, pDCs were incubated 1 h with TGF β and PGE2 inhibitors: TGFBRi = Galunisertib (5 μ M); EPI = EP2 + EP4 inhibitors (10 μ M). Mean values \pm s.e.m are

shown. Source data are provided as a Source Data file and n =minimum 3 independent donors/condition. TGF- β and PGE2 (pg/mL) in SNDIL were quantified by MSD (ND = value not determined). **F** Quantification of IFN- α (pg/mL) by ECLIA multiplex assay in breast (square) and ovarian (triangle) SNDIL containing IFNL1 or not (n = 80 breast & 25 ovarian tumors). TGF β -low and TGF β -high groups were determined using the median value of 475.3 pg/mL (n = 71 breast and 22 ovarian tumors). Mean values \pm s.e.m are shown. Statistical significance was determined using a two-sided t test. **G** GSEA Hallmark analysis showing enriched gene sets in tumor associated pDCs versus blood pDCs RNA sequencing. Tumor-associated pDCs and blood pDCs were sorted from n = 4 breast tumors or 5 healthy PBMCs. Enriched gene sets obtained with the fGSEA R-package were filtered with a $\text{padj} < 0.05$.

NLCR5, involved in the transcriptional regulation of MHC-I is the most significantly upregulated gene, suggesting that the IFN-I secreting phenotype is undoubtedly also associated with an upregulated class-I presentation capacity.

pDCs have been described to lose their IFN- α producing capacity in response to TLR activation in the tumor due to the presence in the TME of TGF- β and TNF- α ¹⁵. Herein, we demonstrated a reversion of the inhibitory effects of TGF- β by IFN-III, though the mechanism involved remains to be explored. One hypothesis is that IFN-III induces a downregulation of TGF β RI as illustrated in our transcriptomic data. IFN-III could also inhibit TGF- β downstream signaling via an intracellular inhibitory factor. Indeed, it was shown that the signaling pathway PI3K/AKT/mTOR could modulate and suppress TGF- β RI-mediated Smad activation^{49,50}. This signaling pathway stimulated by IFN-III could explain how IFN-III prevents pDC inhibition by TGF- β . As other molecules such as lipids (i.e., PGE2), or enzymes (i.e., arginase1, CD73...) present in the TME contribute to the immunosuppressive environment⁵¹, we exposed pDCs to SN-DIL to fully mimic the TME. Strikingly, IFN-III was also able to counteract the inhibitory effect of complete SN-DIL, demonstrating the power of IFN-III to prime pDCs toward an IFN-I phenotype even in a hostile microenvironment. By blocking TGF- β , PGE2, or both molecules, we also observed that the inhibitory effect of SN-DILs is sometimes completely reversed or preferentially restored by one of the blockers, suggesting multiple mechanisms at the origin of pDC inhibition, albeit with a major role for these two compounds. We did not observe any difference between SNDIL from breast or ovary, indicating conserved immunosuppressive pathways in these two tumor types, which remains to be confirmed in other solid tumors.

The immunostimulatory properties of IFN-III-stimulated pDCs are questionable as they upregulated PD-L1 and ICOS-L. ICOS-L induces Treg expansion exclusively in the absence of IFN-I⁵². However, IFN-I attenuates Treg functions in the TME⁵³. Therefore, even if IFN-III-stimulated pDCs express ICOS-L at their surface, their own production of IFN-I may be sufficient to inhibit Treg expansion. Finally, pDCs exposed to IFN-III may secrete such a high dose of IFN-I in response to a TLR agonist that its impact on other immune cells could counteract immunomodulatory effects induced by PD-L1 expression. If T cell anergy induced by PD-L1 expression on IFN-III-stimulated pDCs could be overcome by combining IFN-III with immune checkpoint inhibitors, this could represent a good strategy to bypass PD-L1 immunosuppressive properties. In light of these observations, above the rate of pDCs tumor infiltration, the state of activation of pDCs should be taken in consideration to comment the clinical prognosis. This may reconcile the divergent prognostic impact of pDCs in tumors described in the literature. Further functional assays on purified TA-pDCs could provide insights into the biology of these cells in tumors, but are difficult to set up due to their rarity and the small size of human biopsies. In situ, a proximal ligation assay may help us to visualize this cross-talk. Moreover, the advent of spatial transcriptomic will undoubtedly enable us to improve our understanding of the many cross-talks and pathways that operate within the tumor. Inference of cell-cell

communication between DC subsets in human tumors using the CellChat tool on scRNA seq data may also help us to decipher preferential interactions between pDCs and cDC1s. Alternatively, the use of transgenic mice with pDCs conditionally deleted for IFNL1 may help us to understand this cross-talk in vivo.

Finally, using IMQ (TLR7 agonist), we demonstrated that IFN-III pre-treatment fostered pDCs to respond to suboptimal TLR7 agonist doses. This ability to respond to TLR7 activation at a lower dose could have therapeutic applications. Indeed, TLR7 agonist are well known in the field of skin diseases, as shown by the patient-applied topical cream containing 5% IMQ which is clinically effective and safe in the management of human papillomavirus infections^{54,55}. In cancer, TLR7 agonist have also been described for their anti-tumor properties, with increased mouse survival in pancreatic ductal adenocarcinoma models and promising results in immunotherapy^{56–59}. A clinical study aiming at treating patients with IMQ also showed its ability to induce immune-mediated rejection of skin metastases in breast cancer patients⁵⁹; Thus, TLR7 upregulation in pDCs following IFN-III stimulation could contribute to promote faster IFN- α production without triggering endogenous danger signals and could thus favor tumor control^{4,60}. Furthermore, combining both IFN-III and TLR7 agonist could help to reduce IMQ doses in therapies to avoid side effects while preserving its therapeutic efficacy⁶¹. Consistently, combining TLR3L, able to induce IFN-III, with TLR7L may also be an alternative strategy. Moreover, this combination could also promote the efficacy of TLR7 agonist treatments that have not been sufficiently effective in late-stage clinical trials. An immunocytokine combining IFN-III and anti-PD1 would be also of interest. Finally, based on these observations and as IFN-I is part of cancer treatment history and still used today for severe cases, the role of IFN-III in anti-cancer treatment could be interesting especially since the IFN-III receptor is not ubiquitously expressed compared to IFNAR receptors (IFN-I receptor) and thus could avoid many side effects known to be problematic with IFN- α treatment.

Methods

Human samples and study approval

Healthy human blood (collected in EDTA anticoagulant-containing tubes) was purchased anonymously from the Etablissement Français du Sang (EFS, Lyon, France). Participants were French voluntary donors, not recruited specifically for this study and other population characteristics were not collected. Fresh tumors were obtained from the Biological Resources Center (BRC) of the CLB (BB-0033-00050, Lyon, France) after approval from the Institutional Review Board and Ethics Committee of the Center Léon Bérard (CLB; L-06-36 and L-11-26) and patient-written informed consent, in accordance with the Declaration of Helsinki.

Public transcriptomic data analysis

IFNL1 or *IL10R β* RNA normalized counts were retrieved from the Human Cell Atlas (HCA) to analyze their expression in PBMCs, or were retrieved from the Tumor Immune Single-cell Hub (TISCH) to analyze their expression in tumor-associated immune cells.

Plasmacytoid dendritic cell isolation

PBMCs were isolated using a lymphocyte separation medium (Eurobio Scientific) and a myeloid cell enrichment was obtained with Percoll separation medium (GE Healthcare). Then, plasmacytoid dendritic cells were obtained using the Plasmacytoid Dendritic cell isolation Kit II, human (Miltenyi, Ref: 130-092-207). The blood volume we obtain from EFS is always 450 mL and the number of collected pDCs varies with a mean of $8.4 \times 10^5 \pm 4.5 \times 10^5$ (on $n = 30$ donors). The purity is also always controlled with a mean of $93.5\% \pm 3.2\%$ (including pDCs used for RNAseq experiment) as shown in Supplementary Fig. 10.

Flow cytometry for phenotyping and pSTAT1 quantification

pDCs isolated from PBMCs were treated with or without 100 ng/mL IFN- λ 1/IL-29 (Peprotech - ref: #300-02 L) and/or 20 ng/mL IL-3 (Peprotech - ref: 200-03) for 24 h at 37 °C 5% CO₂. After stimulation, pDCs were stained for 15 min at 4 °C with zombie NIR (1/400, ref: 423106, Biolegend), followed by an antibody staining of 30 min at 4 °C containing: anti-CD123 (ref: 563405, clone: 7G3, BD, diluted 1/100), anti-BDCA2 (ref: 1294661, clone: V24-785, BD, diluted 1/50), anti-PD-L1 (ref: B285480, clone: 29E2A3, Biolegend, diluted: 1/50), anti-ICOS-L (ref: 2017863, clone: MIH12, Invitrogen, diluted 1/50), anti-HLA-DR (ref: B314704, clone: L243, Biolegend, diluted 1/50), anti-CD80 (ref: 7046635, clone: L307.4, BD, diluted: 1/50), anti-CD86 (ref: 93222850, clone: 23331(FUN-1), BD, diluted 1/50). Cells were fixed at RT for 45 min in the dark with FA4% (Sigma-Aldrich - ref: F8775-500ML).

For some experiments, pDCs were stain with anti-TLR7 (R&D, ref: IC5875P, clone: 533707, diluted: 1/100) or anti-TLR9 (Ebioscience, ref: 12-9099-82, clone: eB72-1665).

For pSTAT1 quantification, cell suspensions were treated with 100 ng/mL IFN- λ 1/IL-29 (Peprotech - ref: #300-02 L) or 1,000 U/mL IFN- β (Peprotech - ref: #300-02BC) for 45 min at 37 °C. Cells were then stained with zombie NIR (1/400, ref: 423106, Biolegend) for 20 min at 4 °C and antibody mix containing: anti-BDCA2 (clone: L307.4, BD, diluted 1/50), anti-CD123 (clone: 7G3, BD, diluted: 1/100), anti-HLA-DR (clone: L243, Biolegend, diluted: 1/50), anti-CD3 (clone: UCHT1, BD, diluted: 1/50), anti-CD20 (clone: 2H7, BD, diluted: 1/20), and anti-CD14 (clone: A59, BD, diluted: 1/50). BD Lyse/Fix Buffer (BD 558049) was used to fix cells for 10 min at 37 °C 5% CO₂. This step was followed by a cell permeabilization with Perm Buffer III (BD 558050) for 30 min on ice. Pellets were resuspended in antibody mix containing: anti-pSTAT1 (ref: 612597, clone: 4a, BD, diluted: 1/10), anti-CD11c (clone: Bu15, Biolegend, diluted: 1/20), anti-CD56 (clone: 901, Beckman Colter, diluted: 1/50) and anti-CD45 (clone: HI30, BD, diluted: 1/25) and incubated in the dark at RT for 40 min.

All flow cytometric acquisitions were done on an LSRFortessa Cell Analyzer (BD Biosciences), and data were processed in FlowJo 10.4 (Tristar).

Quantitative real Time RT-PCR

pDCs were incubated for 6 h, 12 h or 18 h with IFN- λ 1 (100 ng/mL) at 37 °C 5% CO₂. pDCs were then lysed with a 1% 2- β -Mercaptoethanol (Sigma-Aldrich, M6250-100ML) + TCL Buffer (Qiagen, 1031576) solution. Total RNAs were then extracted from cultured cells using the single cell RNA purification kit (NORGEN, ref: 51800) according to the manufacturer's instruction. RNA retro-transcription into cDNA was performed with the I Script cDNA Synthesis Kit (BioRad, ref: #172-5038). SsoAdvanced universal SYBR Green super Mix was used for quantitative polymerase chain reaction in real-time. Probe sequences were OAS2 Fw: "5'-AGGGAGTGGCCATAGGTGG-3'", OAS2 Rv: "5'-AACACCTGGATGGTGAACCC-3'". qPCR was performed with CFX Real-Time PCR system machine (BioRad), using the following program: 1 min hold at 95 °C, 39 cycle of 5 s at 90 °C (denaturing) and 10 s at 60 °C (annealing/extension). Each sample was analyzed in duplicate, and the experiments were done twice. A non-template control (RNA-free water) was included on every plate.

RNA Sequencing and analysis

RNA sequencing was performed on untreated or IFN- λ 1 treated (100 ng/mL, 12 h at 37 °C) isolated pDCs (without IL-3). pDCs were lysed with a 1% 2- β -Mercaptoethanol (Sigma-Aldrich, M6250-100ML) + TCL Buffer (Qiagen, 1031576) solution. Total RNAs were then extracted from cultured cells using the single cell RNA purification kit (Norgen Biotek, ref: 51800) according to the manufacturer's instruction. The sequencing and quality controls were then carried out by the Cancer Genomics Platform of the Leon Berard Center (CLB). Data normalization was then done with the DESeq2 R packages. PCA and volcano plots were created with DESeq2 R packages. DEGs between pDCs treated or not with IFN- λ 1 were defined with a $|\log(\text{Foldchange})| > 0.58$ and adjusted p -value < 0.05 and z-scores computed with R studio. A Z-score heatmap of the complete list of DEGs was then uploaded on the Morpheus website created by the Broad Institute. GSEA analysis was performed from the GSEA-MSigB software using the «h.all.v7.5.1.symbols.gmt» gene set. A Venn diagram was created with ggvenn R package on the enriched genes from "Interferon gamma response" and "Interferon alpha response". Normalized counts from specific genes of interest were retrieved from the normalized count table created by DESeq2 and plotted using ggplot2 R package.

pDC activation with Imiquimod or with activated cDC1 supernatant

To assess IMQ suboptimal dose, pDCs isolated from PBMCs were treated with 100 ng/mL IFN- λ 1 and/or IL-3 (20 ng/mL) for 18 h at 37 °C 5% CO₂, and different concentrations of IMQ were added to pDCs culture for 24 h. Cells were then stained for flow cytometric analysis and phenotyping. pDCs were treated with 100 ng/mL IFN- λ 1 for 18 h at 37 °C 5% CO₂, before being activated with the strongest dose (250 ng/mL) or the weakest dose of IMQ (50 ng/mL). pDCs with no prior pre-treatment were kept at 4 °C for 18 h before IMQ activation and named "Medium".

Human cDC1s (CLEC9A + CD141 +) were generated in vitro from CD34+ hematopoietic stem cells obtained from Lymphobank (Besancon, France) according to Kirkling et al.⁶² Briefly, CD34+ cells were amplified with cytokines (FLT3-L, IL-3 and SCF) and differentiated with FLT3-L, GM-CSF, SCF and co-cultured with the OP9-DLL1 cell line. FACS-sorted CD141 + cDC1 (using the anti-CD141 Ab, clone: AD5-14H12, Miltenyi Biotec) were then stimulated with 10 μ g/mL of TLR3 agonist (Poly(I:C) HMW, Invivogen) for 24 h. Then culture supernatants were used to stimulate isolated pDCs 24 h (isolated from PBMCs of healthy patients as previously described). When indicated, pDCs were incubated 1 h with IFNLR1 or/and IFNAR2 blocking antibodies at 5 μ g/mL (Anti-Human IFN-Lambda Receptor 1, Clone MMHLR-1 (Mab), PBL, Ref: 21885 & Anti-Human IFN-Alpha/Beta Receptor Chain 2, Clone MMHAR-2 (Mab), PBL, Ref: 21385) before adding cDC1 supernatants. pDC activation was monitored by FACS using PD-L1 as described above.

pDCs co-culture with TGF- β , PGE2 and/or tumor supernatant (SN-DILs)

pDCs isolated from PBMCs were treated with 100 ng/mL IFN- λ 1 and/or 2 ng/mL of TGF- β (R&D bioscience, ref: #240-B) and/or 10 μ M PGE2 (TOCRIS) or 25% of SN-DILs for 24 h at 37 °C 5% CO₂. pDCs were activated with 50 or 250 ng/mL of IMQ for 24 h. To ensure that pDC viability was maintained throughout the protocol, 20 ng/mL of IL-3 was added when mentioned in the Figure Legends. Supernatants were harvested after culture and kept at -80 °C before conducting electroluminescence assays to dose different cytokines. Cells were stained for 15 min at 4 °C with zombie NIR (1/400, ref: 423106, Biolegend), followed by an antibody staining of 30 min at 4 °C containing: anti-CD123 (ref: 563405, clone: 7G3, BD, diluted: 1/100), anti-BDCA2 (ref: 1294661, clone: V24-785, BD, diluted: 1/50), anti-PD-L1 (ref: B285480, clone: 29E2A3, Biolegend, diluted: 1/50), anti-ICOS-L (ref: 2017863, clone: MIH12, Invitrogen, diluted: 1/50), anti-HLA-DR (ref: B314704, clone: L243, Biolegend, diluted: 1/50), anti-CD80 (ref: 7046635, clone: L307.4,

BD, diluted: 1/50), anti-CD86 (ref: 93222850, clone: 23331(FUN-1), BD, diluted: 1/50). All flow cytometry acquisitions were done on a LSRFortessa Cell Analyzer (BD Biosciences), and data were processed in FlowJo 10.4 (Tristar).

Tumor dilaceration and tumor cell suspensions

Tumors were manually dilacerated in RPMI and supernatants were harvested (referred as SN-DIL). Enzymatic digestion was then performed on dilacerated tumors with DNase I (Sigma, ref: D4513) and 200 U/ml Collagenase IV (Gibco, ref: 17104-019) in 10 mL RPMI 20% FCS for 45 min at 37 °C. The whole solution was filtered on a 70 µm strainer. Single cell suspensions were obtained and used for pSTAT1 staining.

TGF-β and PGE2 receptor inhibition

TGF-β receptors were inhibited with 5 µM of Galunisertib (TORCIS, ref: 6956). PGE2 EP2 and EP4 receptors were specifically inhibited using 10 µM of EP2 and EP4 antagonist obtained from Cayman Chemical (respectively: PF-04418948, ref: 15016 and L-161,982, ref: 10011565). Isolated pDCs were incubated 1 h with inhibitors at the indicated concentration before adding tumor supernatant (SNDIL) and the different pre-treatments as indicated.

RNA-seq analysis of TA-DC subsets

Single-cell suspensions were stained using antibodies listed in Supplementary Table 1 and additional antibody validation informations are available from the manufacturers. Dying cells were excluded by DAPI staining. Lymphocytes, NK cells, neutrophils, and other myeloid cells (monocytes, macrophages, and inflammatory monocytes) were also excluded using anti-CD3, CD56, CD15 and CD14 antibodies, respectively, in the lineage. In the HLA-DR+ Lin- gate, DC subsets were identified using the following phenotypes: CD11c-/low CD123+ pDCs, CD11c+ BDCA1- BDCA3high CLEC9A+ cDC1s, CD11c+ BDCA1+ BDCA3- CD207- cDC2s and CD11c+ BDCA1+ BDCA3- CD207high LC. Using a BD FACSAria III, 1,000 cells of each identified TA-DC subset were then sorted in TCL buffer (Qiagen) supplemented with 1% β-mercaptoethanol (SIGMA) for RNA-seq experiments.

RNA from sorted samples was extracted using a Single Cell RNA Purification Kit (Norgen Biotech), including on-column DNase digestion (Qiagen), as described by the manufacturer's protocol. cDNA was generated with SmartSeqV4 oligodT primer (Takara), following the manufacturer's protocol. The quantity and quality of cDNA were assessed using Qubit dsRNA high sensitivity (ThermoFisher) and DNA HS D5000 (Agilent), respectively. Multiplexed pair-end libraries 50nt in length were obtained using Nextera XT kit (Illumina). Sequencing was performed in the same batch in Illumina NovaSeq 6000 using an average depth of 32 million reads. Library, sequencing and quality control of the sequencing were performed by the genomic platform and the Gilles Thomas bioinformatics platform of the CLB. Reads were mapped to the human genome reference (hg19/GRCh38) using STAR software. Finally, the Salmon tool was used to quantify gene expression as read counts.

Multiplexed immunofluorescence and spatial analysis

We collected formalin-fixed paraffin-embedded (FFPE) tissues (1 slide of 4 µm) from surgical specimens from 10 breast cancer patients at diagnosis. Markers for tumor-infiltrating DC identification were chosen based on previous data from the literature. In particular, we multiplexed, BDCA2 (Goat Polyclonal, R&D Systems, AF1376) for pDCs, XCR1 (Rabbit D2F8T, Cell Signaling, 44665S) for cDC1s, CD8 (Mouse C8/144B, DAKO, M7103) for CD8+ T cells and cytokeratin for breast cancer cells. We then used the tyramide-signal amplification (TSA)-based Opal Automation Research Detection Kit (Leica, DS9777) on the Bond RX automatic stainer (Leica Biosystems). Secondary antibodies used to amplify the signal included the Anti-Goat IgG HORSERADISH

Peroxidase (HRP) Conjugated (Donkey Polyclonal, Life Technologies, A16005), the Anti-Rabbit IgG, horseradish Peroxidase (HRP) Conjugated (Goat Polyclonal, Life Technologies, A1604) and the Anti-Rat IgG, HORSERADISH Peroxidase (HRP) Conjugated (Goat Polyclonal, Thermo Scientific, 31470). Different antigen retrieval reagent conditions, antibody concentrations and time of incubation were tested for each marker of interest on tonsil FFPE samples and validated on breast tumors.

After image acquisition, tissue and cell segmentation was performed with Inform Software. Cell coordinates were then retrieved with the Inform data frame, and 2D projections were made with R studio. We then used SPIAT (R) in order to calculate cell distance between pDCs and cDC1s.

Cytokine and chemokine quantification by Meso Scale Discovery (MSD) assay and ECLIA technology

In pDCs co-culture, IFN-α2, IFN-β, TNF-α, IL-6, MIP1-β, CXCL10, CCL19, IL-8 cytokines and chemokines were quantified in pDCs culture using the MSD technology. Quantifications were performed according to the U-plex protocol following manufacturer's instructions and acquired with the MESO QuickPlex SQ 120 instrument.

In breast SNDILs (*n* = 91 breast and 25 ovarian tumors), the following cytokines and chemokines were quantified using ECLIA technology (BioPlex Pro human cytokine, BIORAD): IL-10 (LOD: 0.69 pg/mL), TNF-α (LOD: 1.13 pg/mL), IFN-α2a (LOD: 0.46 pg/mL), IFN-λ1 (LOD: 2.62 pg/mL), and (TGF-β1; LOD: 3.9 pg/mL) was quantified by the same technique. SNDILs used for pDC inhibition experiments (*n* = 12 breast and 7 ovary) were quantified again by MSD technology and PGE2 concentrations were analyzed by ELISA (Cayman chemicals, ref 514010).

Statistics

Statistical analyses were performed using Prism Version 9.0 (GraphPad Software) for the Friedman test, and XLSTAT add-on on Excel software for the Kruskal-Wallis test. The Friedman non-parametric test was used to compare paired values corresponding to each blood/tumor donor, otherwise we used the Kruskal-Wallis test. Statistical significance: **p* < 0.05, ***p* < 0.01, ****p* < 0.001, and *****p* < 0.0001. Each graphical representation reflects the associated non-parametric statistical test. No statistical analysis was performed when the number of samples was ≤ 3.

Reporting summary

Further information on research design is available in the Nature Portfolio Reporting Summary linked to this article.

Data availability

Source data are provided with this paper. RNA sequencing data that support some findings of this study have been deposited in Gene Expression Omnibus – NCBI (GEO) with the GEO ID [GSE237879](https://www.ncbi.nlm.nih.gov/geo/query/acc.cgi?acc=GSE237879). Source data are provided with this paper.

Code availability

All codes used for analysis in this study were based on the following R packages and Github link: - DESeq2 (10.18129/B9.bioc.DESeq2): <https://github.com/thevelab/DESeq2> - msigdb (10.18129/B9.bioc.msigdb): <https://davislaboratory.github.io/msigdb> - tidyverse (<https://tidyverse.org>): <https://github.com/tidyverse> - dplyr (10.32614/CRAN.package.dplyr): <https://github.com/tidyverse/dplyr> - fgsea (10.18129/B9.bioc.fgsea): <https://github.com/ctlab/fgsea> - ggplot2 (10.32614/CRAN.package.ggplot2): <https://github.com/tidyverse/ggplot2> - SPIAT (10.18129/B9.bioc.SPIAT): <https://trigosteam.github.io/SPIAT> All bioinformatic tools and methods used in this manuscript have been published previously and no custom code was used. For further information please contact the corresponding author.

References

- Cella, M. et al. Plasmacytoid monocytes migrate to inflamed lymph nodes and produce large amounts of type I interferon. *Nat. Med.* **5**, 919–923 (1999).
- Siegal, F. P. et al. The nature of the principal type 1 interferon-producing cells in human blood. *Science* **284**, 1835–1837 (1999).
- Gresser, I. & Belardelli, F. Endogenous type I interferons as a defense against tumors. *Cytokine Growth Factor Rev.* **13**, 111–118 (2002).
- Zitvogel, L., Galluzzi, L., Kepp, O., Smyth, M. J. & Kroemer, G. Type I interferons in anticancer immunity. *Nat. Rev. Immunol.* **15**, 405–414 (2015).
- Asmana Ningrum, R. Human interferon alpha-2b: a therapeutic protein for cancer treatment. *Sci. (Cairo)* **2014**, 970315 (2014).
- Gajewski, T. F., Schreiber, H. & Fu, Y.-X. Innate and adaptive immune cells in the tumor microenvironment. *Nat. Immunol.* **14**, 1014–1022 (2013).
- Sprooten, J., Agostinis, P. & Garg, A. D. Type I interferons and dendritic cells in cancer immunotherapy. *Int Rev. Cell Mol. Biol.* **348**, 217–262 (2019).
- Katlinksi, K. V. et al. Inactivation of interferon receptor promotes the establishment of immune privileged tumor microenvironment. *Cancer Cell* **31**, 194–207 (2017).
- Castiello, L. et al. Disruption of IFN-I signaling promotes HER2/Neu tumor progression and breast cancer stem cells. *Cancer Immunol. Res.* **6**, 658–670 (2018).
- Hubert, M., Gobbi, E., Bendriss-Vermare, N., Caux, C. & Valladeau-Guilemond, J. Human tumor-infiltrating dendritic cells: from in situ visualization to high-dimensional analyses. *Cancers (Basel)* **11**, (2019).
- Labidi-Galy, S. I. et al. Quantitative and functional alterations of plasmacytoid dendritic cells contribute to immune tolerance in ovarian cancer. *Cancer Res.* **71**, 5423–5434 (2011).
- Sisirak, V. et al. Impaired IFN- α production by plasmacytoid dendritic cells favors regulatory T-cell expansion that may contribute to breast cancer progression. *Cancer Res.* **72**, 5188–5197 (2012).
- Hartmann, E. et al. Identification and functional analysis of tumor-infiltrating plasmacytoid dendritic cells in head and neck cancer. *Cancer Res.* **63**, 6478–6487 (2003).
- Bekeredjian-Ding, I. et al. Tumour-derived prostaglandin E2 and transforming growth factor- β synergize to inhibit plasmacytoid dendritic cell-derived interferon- α . *Immunology* **128**, 439–450 (2009).
- Sisirak, V. et al. Breast cancer-derived transforming growth factor- β and tumor necrosis factor- α compromise interferon- α production by tumor-associated plasmacytoid dendritic cells. *Int J. Cancer* **133**, 771–778 (2013).
- Fabricius, D. et al. Prostaglandin E2 inhibits IFN- α secretion and Th1 costimulation by human plasmacytoid dendritic cells via E-prostanoid 2 and E-prostanoid 4 receptor engagement. *J. Immunol.* **184**, 677–684 (2009).
- Chakraborty, S. et al. Application of toll-like receptors (TLRs) and their agonists in cancer vaccines and immunotherapy. *Front. Immunol.* **14**, 1227833 (2023).
- Hubert, M. et al. IFN-III is selectively produced by cDC1 and predicts good clinical outcome in breast cancer. *Sci. Immunol.* **5**, eaav3942 (2020).
- Lazear, H. M., Schoggins, J. W. & Diamond, M. S. Shared and distinct functions of type I and Type III interferons. *Immunity* **50**, 907–923 (2019).
- Au-Yeung, N., Mandhana, R. & Horvath, C. M. Transcriptional regulation by STAT1 and STAT2 in the interferon JAK-STAT pathway. *JAK-STAT* **2**, e23931 (2013).
- Finotti, G., Tamassia, N., Calzetti, F., Fattovich, G. & Cassatella, M. A. Endogenously produced TNF- α contributes to the expression of CXCL10/IP-10 in IFN- λ 3-activated plasmacytoid dendritic cells. *J. Leukoc. Biol.* **99**, 107–119 (2016).
- Finotti, G., Tamassia, N. & Cassatella, M. A. Synergistic production of TNF α and IFN α by human pDCs incubated with IFN λ 3 and IL-3. *Cytokine* **86**, 124–131 (2016).
- Megjugorac, N. J., Gallagher, G. E. & Gallagher, G. Modulation of human plasmacytoid DC function by IFN-lambda1 (IL-29). *J. Leukoc. Biol.* **86**, 1359–1363 (2009).
- Syedbasha, M. et al. Interferon- λ enhances the differentiation of naive B cells into plasmablasts via the mTORC1 pathway. *Cell Rep.* **33**, 108211 (2020).
- Cao, W. et al. Toll-like receptor-mediated induction of type I interferon in plasmacytoid dendritic cells requires the rapamycin-sensitive PI(3)K-mTOR-p70S6K pathway. *Nat. Immunol.* **9**, 1157–1164 (2008).
- Guiducci, C. et al. PI3K is critical for the nuclear translocation of IRF-7 and type I IFN production by human plasmacytoid predendritic cells in response to TLR activation. *J. Exp. Med.* **205**, 315–322 (2008).
- Lee, B. L. et al. UNC93B1 mediates differential trafficking of endosomal TLRs. *Elife* **2**, e00291 (2013).
- Kawasaki, T. & Kawai, T. Toll-like receptor signaling pathways. *Front. Immunol.* **5**, 461 (2014).
- Graustein, A. D. et al. Toll-like receptor chaperone HSP90B1 and the immune response to Mycobacteria. *PLoS One* **13**, e0208940 (2018).
- Wang, Y. et al. The autoimmunity-associated gene PTPN22 potentiates toll-like receptor-driven, type 1 interferon-dependent immunity. *Immunity* **39**, 111–122 (2013).
- Grzes, K. M. et al. Plasmacytoid dendritic cell activation is dependent on coordinated expression of distinct amino acid transporters. *Immunity* **54**, 2514–2530.e7 (2021).
- Troutman, T. D. et al. Role for B-cell adapter for PI3K (BCAP) as a signaling adapter linking Toll-like receptors (TLRs) to serine/threonine kinases PI3K/Akt. *Proc. Natl Acad. Sci. USA* **109**, 273–278 (2012).
- Guo, H. et al. SCARB2/LIMP-2 regulates IFN production of plasmacytoid dendritic cells by mediating endosomal translocation of TLR9 and nuclear translocation of IRF7. *J. Immunol.* **194**, 4737–4749 (2015).
- Kobayashi, T. et al. Human SLC15A4 is crucial for TLR-mediated type I interferon production and mitochondrial integrity. *Int Immunol.* **33**, 399–406 (2021).
- Talukder, A. H. et al. Phospholipid Scramblase 1 regulates Toll-like receptor 9-mediated type I interferon production in plasmacytoid dendritic cells. *Cell Res.* **22**, 1129–1139 (2012).
- Dougan, M., Dranoff, G. & Dougan, S. K. GM-CSF, IL-3, and IL-5 family of cytokines: regulators of inflammation. *Immunity* **50**, 796–811 (2019).
- Alcumbre, S. G. et al. Diversification of human plasmacytoid predendritic cells in response to a single stimulus. *Nat. Immunol.* **19**, 63–75 (2018).
- Sisirak, V. et al. Breast cancer-derived transforming growth factor- β and tumor necrosis factor- α compromise interferon- α production by tumor-associated plasmacytoid dendritic cells. **133**, 771–778 (2013).
- Broggi, A., Tan, Y., Granucci, F. & Zanoni, I. IFN- λ suppresses intestinal inflammation by non-translational regulation of neutrophil function. *Nat. Immunol.* **18**, 1084–1093 (2017).
- Duong, F. H. T. et al. IFN- λ receptor 1 expression is induced in chronic hepatitis C and correlates with the IFN- λ 3 genotype and with nonresponsiveness to IFN- α therapies. *J. Exp. Med.* **211**, 857–868 (2014).

41. Ngo, C., Garrec, C., Tomasello, E. & Dalod, M. The role of plasmacytoid dendritic cells (pDCs) in immunity during viral infections and beyond. *Cell Mol. Immunol.* **21**, 1008–1035 (2024).
42. Abbas, A. et al. The activation trajectory of plasmacytoid dendritic cells in vivo during a viral infection. *Nat. Immunol.* **21**, 983–997 (2020).
43. Ghirelli, C., Zollinger, R. & Soumelis, V. Systematic cytokine receptor profiling reveals GM-CSF as a novel TLR-independent activator of human plasmacytoid predendritic cells. *Blood* **115**, 5037–5040 (2010).
44. Grouard, G. et al. The enigmatic plasmacytoid T cells develop into dendritic cells with interleukin (IL)-3 and CD40-ligand. *J. Exp. Med.* **185**, 1101–1111 (1997).
45. Ito, T. et al. Plasmacytoid dendritic cells regulate Th cell responses through OX40 ligand and type I IFNs. *J. Immunol.* **172**, 4253–4259 (2004).
46. Ito, T. et al. Differential regulation of human blood dendritic cell subsets by IFNs. *J. Immunol.* **166**, 2961–2969 (2001).
47. Aspor, C., Leccia, M.-T., Charles, J. & Plumas, J. Plasmacytoid dendritic cells support melanoma progression by promoting Th2 and regulatory immunity through OX40L and ICOSL. *Cancer Immunol. Res.* **1**, 402–415 (2013).
48. Hosokawa, Y., Hosokawa, I., Shindo, S., Ozaki, K. & Matsuo, T. IL-29 enhances CXCL10 production in TNF- α -stimulated human oral epithelial cells. *Immunological Investig.* **46**, 615–624 (2017).
49. Yu, J. S. L. et al. PI3K/mTORC2 regulates TGF- β /Activin signalling by modulating Smad2/3 activity via linker phosphorylation. *Nat. Commun.* **6**, 7212 (2015).
50. Song, K., Wang, H., Krebs, T. L. & Danielpour, D. Novel roles of Akt and mTOR in suppressing TGF- β /ALK5-mediated Smad3 activation. *EMBO J.* **25**, 58–69 (2006).
51. De Martino, M., Rathmell, J. C., Galluzzi, L. & Vanpouille-Box, C. Cancer cell metabolism and antitumour immunity. *Nat. Rev. Immunol.* **24**, 654–669 (2024).
52. Faget, J. et al. ICOS-ligand expression on plasmacytoid dendritic cells supports breast cancer progression by promoting the accumulation of immunosuppressive CD4⁺ T Cells. *Cancer Res.* **72**, 6130–6141 (2012).
53. Gangaplara, A. et al. Type I interferon signaling attenuates regulatory T cell function in viral infection and in the tumor micro-environment. *PLoS Pathog.* **14**, e1006985 (2018).
54. Garland, S. M. Imiquimod. *Curr. Opin. Infect. Dis.* **16**, 85–89 (2003).
55. Urošević, M. & Dummer, R. Role of imiquimod in skin cancer treatment. *Am. J. Clin. Dermatol.* **5**, 453–458 (2004).
56. Michaelis, K. A. et al. The TLR7/8 agonist R848 remodels tumor and host responses to promote survival in pancreatic cancer. *Nat. Commun.* **10**, 4682 (2019).
57. Schön, M. P. & Schön, M. TLR7 and TLR8 as targets in cancer therapy. *Oncogene* **27**, 190–199 (2008).
58. Le Mercier, I. et al. Tumor promotion by intratumoral plasmacytoid dendritic cells is reversed by TLR7 ligand treatment. *Cancer Res.* **73**, 4629–4640 (2013).
59. Adams, S. et al. Topical TLR7 agonist imiquimod can induce immune-mediated rejection of skin metastases in patients with breast cancer. *Clin. Cancer Res.* **18**, 6748–6757 (2012).
60. Ferrantini, M., Capone, I. & Belardelli, F. Interferon-alpha and cancer: mechanisms of action and new perspectives of clinical use. *Biochimie* **89**, 884–893 (2007).
61. Bubna, A. K. Imiquimod - Its role in the treatment of cutaneous malignancies. *Indian J. Pharm.* **47**, 354–359 (2015).
62. Kirkling, M. E. et al. Notch signaling facilitates in vitro generation of cross-presenting classical dendritic cells. *Cell Rep.* **23**, 3658–3672.e6 (2018).

Acknowledgements

We wish to thank the staff of the core facilities at the Cancer Research Center of Lyon (CRCL) for technical assistance and the BRC of the CLB for providing human samples, as well as N. Gadot and the research anatomopathology platform of the CLB and the Ex vivo Platform (S. Leon). We thank T. Andrieu, P. Battiston-Montagne, and A. Jambon for assistance in flow cytometry in the CRCL Cytometry platform. We thank Brigitte Manship for the reading and editing of the manuscript. We thank the genomic platform for RNAseq generation (S. Boyault). We thank J. Berthet and C. Dubois for their help and technical advices. As citations were limited, we were unable to cite all available studies, and so apologize to any authors who feel their studies were not adequately represented in our accounting. This work was supported by funding from INSERM (for CS, AS, CR, MA, LM, ACD, EG, AV, LB, LL, SD, MH, NBV, CC and JVG), INCA (PLBIO INCa_4508 and PLBIO INCa_11155; for CS, AS, ACD, EG, AV, MH, NBV, CC and JVG), ARC Foundation for MH, Ligue contre le Cancer (Nationale, Régionale Auvergne-Rhône-Alpes et Saône-et-Loire, Comité de la Savoie; for CS, AS, ACD, EG, MH, NBV, CC and JVG), and the Région Rhône-Alpes Auvergne (IRICE; for CS, AS, ACD, EG, AV, MH, NBV, CC and JVG). We would like to thank the ESMO for E. Gobbi (any views, opinions, findings, conclusions or recommendations expressed in this material are those solely of the authors and do not necessarily reflect those of ESMO), SIRIC project (LYRIC, grant no. INCa_4664) and the FP7 European TumAdoR project (grant no. 602200) for CR and CC, the LABEX DEVweCAN (ANR-10-LABX-0061) of the University of Lyon, within the program “Investissements d’Avenir” organized by the French National Research Agency (ANR), for ACD, NBV, CC and JVG.

Author contributions

C.S. and A.S. designed and performed experiments, did bioinformatics, analyzed results, did statistical analyses, and wrote the manuscript. C.R., A.C.D., L.B., and L.M. designed and performed some experiments, analyzed results, and did statistical analyses. M.A. performed the alignment and the QC of our RNA sequencing data. M.H. provided the RNA sequencing analysis and GSEA pipeline that was used and modified to fit samples and analysis. A.C.D. performed all the mIF staining and E.G. developed the machine learning algorithm with Inform Software. JB performed PGE2 analysis. S.D., L.L., N.B.V., and A.V. provided strategic advice and/or revised the manuscript. C.C. provided strategic advice and revised the manuscript. J.V.G. designed experiments, supervised the research, and wrote the manuscript.

Competing interests

The authors declare no competing interests.

Additional information

Supplementary information The online version contains supplementary material available at <https://doi.org/10.1038/s41467-025-58220-8>.

Correspondence and requests for materials should be addressed to Jenny Valladeau-Guilemond.

Peer review information *Nature Communications* thanks Lucia Gabriele, Daniel Schnepf and the other anonymous reviewer for their contribution to the peer review of this work. A peer review file is available.

Reprints and permissions information is available at <http://www.nature.com/reprints>

Publisher’s note Springer Nature remains neutral with regard to jurisdictional claims in published maps and institutional affiliations.

Open Access This article is licensed under a Creative Commons Attribution-NonCommercial-NoDerivatives 4.0 International License, which permits any non-commercial use, sharing, distribution and reproduction in any medium or format, as long as you give appropriate credit to the original author(s) and the source, provide a link to the Creative Commons licence, and indicate if you modified the licensed material. You do not have permission under this licence to share adapted material derived from this article or parts of it. The images or other third party material in this article are included in the article's Creative Commons licence, unless indicated otherwise in a credit line to the material. If material is not included in the article's Creative Commons licence and your intended use is not permitted by statutory regulation or exceeds the permitted use, you will need to obtain permission directly from the copyright holder. To view a copy of this licence, visit <http://creativecommons.org/licenses/by-nc-nd/4.0/>.

© The Author(s) 2025